Republic of Algeria Democratic and Popular Republic

Ministry of Higher Education and Scientific Research

Echahid Hamma Lakhdar University of El-Oued

Faculty of Science and Technology

Department: Electrical Engineering

Graduation Thesis

Submitted in Partial Fulfillment of the Requirements for the Degree of

Academic Master's Degree

Field: Science and Technology

Electrical control

Specialty: Electrical control

Presented by: ALI BACI AND DJAFAR MEDEKHEL

Topic

Study and implementation of a sliding mode control algorithm for a photovoltaic system powering a pump

Before the jury composed of:

Pr. ALLAG Abdulkarim	**Université Echahid Hamma Lakhdar**	**Chairman**
Dr.Mohammed idris babaarbi	**Université Echahid Hamma Lakhdar**	**Examiner**
Dr.Meriem ALLAG	**Université Echahid Hamma Lakhdar**	**Supervised**

2023-2024

Abstract

This thesis focuses on improving the performance and efficiency of a photovoltaic system through the use of an appropriate algorithm for power interface control. The main objective is to find an effective and optimal sliding mode control algorithm or law allowing to extract the maximum available power from the photovoltaic generator (PVG). Additionally, it involves the study, design, and implementation of a unit combining an MPPT algorithm and the management of energy transmitted to the load (DC electrical machine or alternative machine). The key points addressed in this study include: modeling of a photovoltaic system, topological study of the power interface, study of a maximum power point tracking algorithm, simulation of an MPPT converter.

Keywords: PV (Photovoltaic), DC-DC converter, Modeling, MPPT (Maximum Power Point Tracking), P&O (Perturb and Observe), Sliding mode, MAS (Modeling and Simulation), DC machine

Résumé

Cette thèse est centrée sur l'amélioration des performances et du rendement d'un système

photovoltaïque à travers l'utilisation d'un algorithme approprié pour la commande de l'interface de puissance.L'objectif principal est de trouver un algorithme ou une loi de commande par Mode glissant efficace et optimale permettant d'extraire le maximum de puissance disponible à partir du générateur photovoltaïque (GPV). Ajoutons à cela, l'étude, la conception et la réalisation d'une unité regroupant un algorithme MPPT et la gestion de l'énergie transmise à la charge (Machine électrique DC ou Machine alternative). Les points essentiels traités dans cette étude sont : la modélisation d'un système photovoltaïque, l'étude topologique de l'interface de puissance, l'étude d'un algorithme de poursuite du point

de puissance maximale, la simulation d'un convertisseur MPPT,

Mots-clés : PV (Photovoltaïque), MPPT (Suivi du Point de Puissance Maximale), P&O (Perturbation et Observation),MAS (Modélisation et Simulation),DC (Direct Courant)

ملخص

تركز هذه الأطروحة على تحسين أداء وكفاءة نظام الطاقة الشمسية الكهروضوئية من خلال استخدام خوارزمية مناسبة للتحكم في واجهة الطاقة. الهدف الرئيسي هو إيجاد خوارزمية تحكم انزلاقي فعالة ومثلى أو قانون يسمح باستخراج أقصى طاقة متاحة من المولد الكهروضوئي .(PVG) بالإضافة إلى ذلك، تتضمن الدراسة تصميم وتنفيذ وحدة تجمع بين خوارزمية تتبع نقطة القدرة القصوى (MPPT) وإدارة الطاقة المنقولة إلى الحمل (آلة كهربائية تيار مستمر أو آلة بديلة). تشمل النقاط الرئيسية التي تم تناولها في هذه الدراسة: نمذجة نظام الطاقة الكهروضوئية، دراسة طوبولوجية لواجهة الطاقة، دراسة خوارزمية تتبع نقطة القدرة القصوى، ومحاكاة لمحول.MPPT

الكلمات المفتاحية: الطاقة الشمسية الكهروضوئية، محول DC-DC، النمذجة، تتبع نقطة القدرة القصوى (MPPT)، خوارزمية الاضطراب والمراقبة (P&O)، التحكم الانزلاقي، النمذجة والمحاكاة (MAS)، آلة التيار المستمر.

Nomenclature

PR Standard performance ratio

PVG Photovoltaic Generation

Ppv Total PV power produced (W)

Nps Number of panels in series

Npp Number of panels in parallel

MPPT Maximum Power Point Tracking

AM Air Mass

PV Photovoltaic

DC Direct current

AC Alternating current

MPPT Maximum Power Point Tracking

INC Incremental conductance

MPP Maximum power point

MOSFET Metal oxide semiconductor field effect transistor

I_{ph} Photo current(A) Ish

Isc Short circuit current(A) Isc

Ki Short circuit current of cell at 25 °C and 1000 w/m² Isc 0.0032

T Operating temperature (K) T

Tn Nominal temperature (K)

G Solar irradiance (W/m²) G

Ro Resistance of the load (Ω)

℃ Degree Celsius C Capacitor (μF)

d Diode L Inductor (H)

R Resistor (Ω)

$\boldsymbol{\mu}$F Microfarad

Ω Ohm

t Time (s)

s Second

V Voltage

π Pi

% Percentage

V Voltage

I Current

L Inductance

K Kelvin

E Energy

C Capacitance

$\boldsymbol{\mu}$ m Micrometre

λ Wavelength

c Speed of light

h Plank's constant

$\boldsymbol{\beta}$ Zenith angle (degree (◦))

H2O Water

CO2 Carbon dioxide gas

nm Nanometre

W/m^2 Watt per square metre

$KWh/m^2/day$ Kilowatt-hour per square meter per day

°F Fahrenheit

Iph Generated current due to sunlight irradiation

Id Current through a diode

Rs Resistor in series

Rp Resistor in parallel

Ip Parallel Resistor current

Vt Thermal Voltage

Isc Short circuit current

Voc Open circuit voltage

Pmax Maximum Power

Imax Maximum current

Vmpp Voltage at maximum point

Imp Current at maximum point

Is Diode reverse saturation current (A)

q Diode ideality factor

Rp Shunt resistance (Ω)

K Boltzman constant

q Electron charge = (1,602.10-19 C)

T Temperature in Kelvin (K)

g Gate terminal of the MOSFET

d Grain terminal of the MOSFET

s Source terminal of the MOSFET

q Electron charge (C) =(1.6*10-19)

Voc Open circuit voltage (V) Voc

n The ideality factor of the diode 1.3

K Boltzmann's constant (J/K) 1.38*10-23

Ego Band gap energy of the semiconductor (eV) 1.1

Ns Number of PV cells connected in series Ns

Np Number of PV cells connected in parallel Np

Rs Series resistance (Ω)

Rsh shunt resistance (Ω)

V_t Diode thermal voltage (V) ……

List of Figures

List of Tables

Table of Contents

Chapter II: Modeling of the Photovoltaic System

Chapter III: Analysis and Design of Maximum Power Point Tracking (MPPT) Algorithm

General Introduction

General introduction

Solar energy is one of the most critical and rapidly expanding renewable energy sources globally. Solar technology primarily relies on photovoltaic (PV) cells, which convert sunlight directly into electrical energy through a process known as the photovoltaic effect. This technology offers a clean and sustainable power source, making it an ideal solution to address the environmental and economic challenges associated with the intensive use of fossil fuels.

Research into photovoltaic systems and direct current (DC) machines is not merely an examination of technical advancements; it is also a deep study of integrating these systems into practical applications. Historically, the roots of photovoltaic energy trace back to 1839 when French physicist Edmond Becquerel discovered the photovoltaic effect. Since then, PV cells have evolved from mere laboratory tools to highly efficient units widely used in satellites, residential buildings, industrial applications, and large-scale electrical systems.

Chapter 1 provides a comprehensive overview of photovoltaic systems and DC machines, outlining the fundamental, historical, and technical aspects of these technologies. It reviews the development of PV cell technologies and their operational mechanisms, alongside significant advancements over the years. This chapter also highlights the importance of DC machines in converting electrical energy into mechanical energy and their extensive industrial applications. The evolution of PV cells from initial laboratory experiments to their current widespread use underscores the transformative impact of this technology.

Chapter 2 focuses on the modeling of photovoltaic cells, starting from the ideal model and moving to more complex models that consider various cell configurations and the effects of environmental factors such as temperature and solar radiation on their performance. This chapter analyzes the properties of materials used in PV cell manufacturing, including monocrystalline and polycrystalline silicon, and other semiconductors. Detailed modeling helps

in understanding the performance characteristics and efficiency of different PV cell types under varying conditions. This section also explores the physics behind the photovoltaic effect and how it is harnessed in various cell designs.

Chapter 3 explores the connections of photovoltaic cells, including direct connections and connections through adaptation stages. This chapter explains how to achieve optimal performance of PV cells by improving their connections and using electronic power converters such as DC-DC converters. It delves into Maximum Power Point Tracking (MPPT) techniques in detail, illustrating how to achieve higher efficiency in converting solar energy into usable electrical power. The discussion covers various MPPT algorithms and their implementations in real-world PV systems, emphasizing the importance of these techniques in maximizing the energy output of PV installations.

Chapter 4 introduces the principle of sliding mode control (SMC) and its applications to photovoltaic systems. SMC is an advanced control technique that enables rapid and stable system response to environmental changes and other variables. This chapter elaborates on the benefits of using SMC in PV systems, including enhanced energy efficiency and system stability. It also addresses the challenges of implementing SMC and strategies for overcoming these challenges. The integration of SMC into PV systems is discussed with case studies and examples demonstrating its effectiveness in real-world scenarios. This chapter also compares SMC with other control techniques, highlighting its unique advantages.

This study aims to provide a comprehensive understanding of photovoltaic technologies and DC machines, exploring how their integration can improve energy efficiency and reduce reliance on traditional non-renewable sources. By reviewing the fundamental principles and recent advancements in this field, the research aspires to offer practical solutions to current and future energy problems. The detailed examination of PV cell modeling, connection techniques,

and advanced control methods like sliding mode control underscores the potential of these technologies in creating a more sustainable energy landscape. This research hopes to contribute to the ongoing development of renewable energy technologies and their implementation in various sectors, promoting a cleaner and more sustainable future.

Chapter I

Overview of Photovoltaic Systems and Direct Current Machines (DCM)

I.1. Introduction

Photovoltaic solar energy involves directly producing electricity from light using solar panels. This form of energy is already being utilized in many countries, especially in areas or regions lacking conventional energy resources such as hydrocarbons or coal.

This chapter is dedicated to the fundamental concepts of photovoltaic energy and the description of semiconductors.

I.2. Photovoltaic Energy

Photovoltaic energy stems from the conversion of sunlight into electricity. This conversion occurs within semiconductor materials, which have the property of releasing their charge carriers under external excitation.

The discovery of this light-to-electricity conversion, known as the photovoltaic effect, dates back to 1839 when the Frenchman Edmond Becquerel identified it [1], [2]. He observed the emergence of an electrical potential between two electrodes when they were illuminated.

The term "photovoltaic" originates from the Greek word "phôtos," meaning light (photon), and "Volta," the name of the Italian physicist who discovered the electric battery in 1800 [1], [3].

I.3. Historical Overview

Here are some significant dates in the field of photovoltaic energy:

1839 :French physicist Edmond Becquerel discovers the photovoltaic effect.

1875 :Werner Von Siemens presents an article on the photovoltaic effect in semiconductors to the Berlin Academy of Sciences.

1954 :Three American researchers, Chapin, Peason, and Prince, manufacture a photovoltaic cell.

1958 :The first satellites powered by solar cells are sent into space; one cell achieves a 9% efficiency rate.

1973 :The first house powered by photovoltaic cells is built at the University of Delaware.

1983 :The first solar-powered car travels 4000 km in Australia.[4]

I.4. Semiconductors

Photovoltaic conversion is carried out using semiconductor materials, which are materials whose conductivity is intermediate between conductors and insulators. This conductivity depends heavily on temperature. A semiconductor is a material where the outer electrons are distributed between two energy bands (the conduction band and the valence band), separated by an energy gap, known as the "bandgap," of about a few eV. There are several semiconductors such as silicon (Si), germanium (Ge), selenium (Se), as well as semiconductor compounds like gallium arsenide (GaAs) and cadmium telluride (CdTe).

I.4.1 Silicon

Silicon is the most commonly used semiconductor material for manufacturing microelectronic devices and photovoltaic cells.

Silicon exists in various forms:

- Multicrystalline and monocrystalline forms for bulk layers,
- Amorphous and polycrystalline forms for thin layers.

These different forms are distinguished by their layer thickness and grain size. We will briefly describe their production methods and indicate their efficiency, particularly in the field of photovoltaic conversion.

I.4.2 Silicon Doping

Doping involves implanting impurities into an intrinsic semiconductor to control its electrical properties. The doping technique increases the density of charge carriers within the semiconductor material. Silicon atoms 'Si' have four valence electrons, each bound to a neighboring 'Si' atom by a covalent bond.

a) N-Type Doping

If an atom with five valence electrons (such as phosphorus (P), arsenic (As), or antimony (Sb)) is incorporated into the crystalline lattice, then this atom will have four covalent bonds and one free electron. This weakly bound electron can be easily excited into the conduction band. In this type of material, the number of electrons exceeds the number of holes.

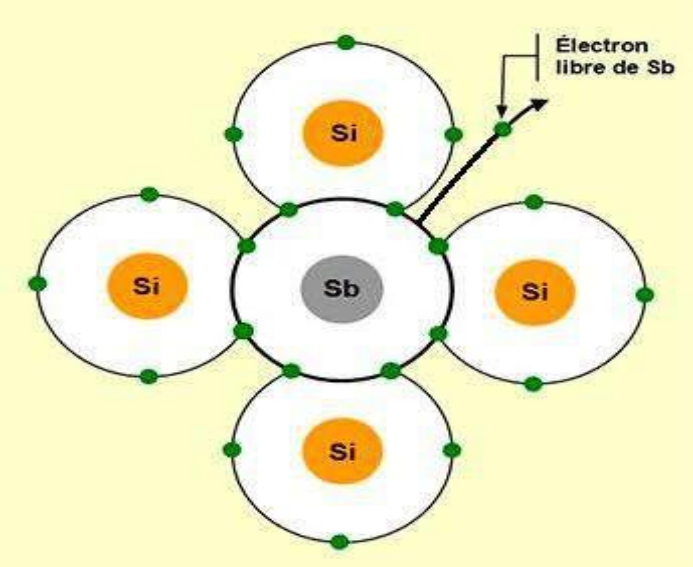

Figure I.1: N-Type Semiconductor

b) P-Type Doping

If a trivalent atom (such as boron **B**) is substituted for a silicon atom in the crystalline lattice, then one electron will be missing for one of the four covalent bonds of the adjacent silicon

atoms. The trivalent atom can accept an electron to complete this fourth bond, thus forming a hole. When the doping is sufficient, the number of holes exceeds the number of electrons.

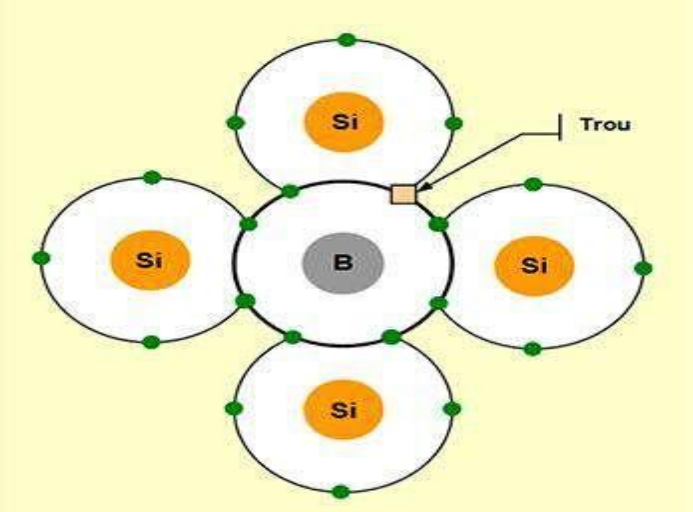

Figure I.2: P-Type Doping

c) P-N Junction

The P-N junction is the basis of most semiconductor applications. It is created by contacting a P-type semiconductor and an N-type semiconductor (in theory). In the contact region, the free electrons from the N segment penetrate into the P segment and recombine with the holes. Similarly, the holes from the P segment penetrate into the N segment and recombine with the electrons [5].

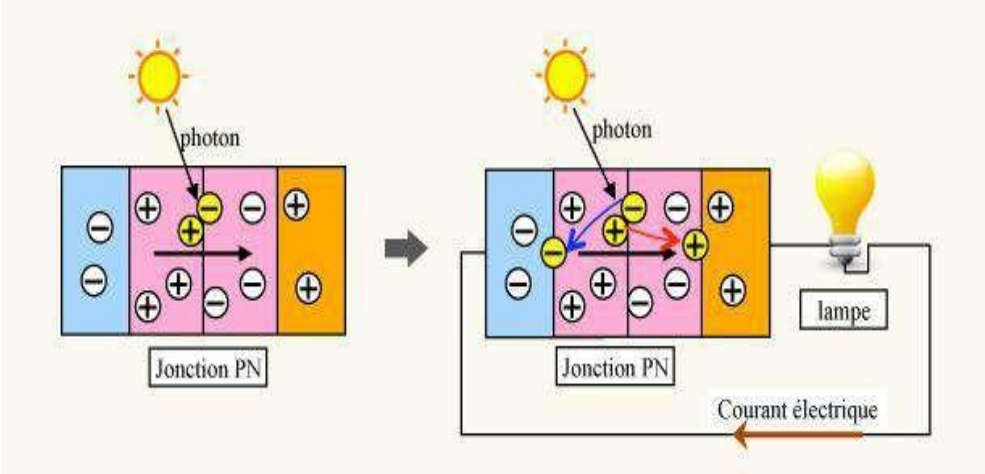

Figure I.3: P-N Junction

I.5. Photovoltaic Conversion

Photovoltaic conversion involves transforming solar energy into electrical energy. This transformation is based on the following three mechanisms:

- Absorption of light in the material (photons with energy ($E.\lambda = hc$) greater than that associated with the bandgap Eg).
- Conversion of photon energy into electrical energy, corresponding to the creation of electron-hole pairs in the space charge region: electrons move towards the P region, holes towards the N region, resulting in a generation photocurrent. In the N or P region, minority carriers generate a diffusion photocurrent. These two currents add up to give a resulting photocurrent Iph.
- Collection of generated charges in the device; achieved through the metallic contacts of the P and N regions (cathode and anode) [1].

I.6. Solar Radiation

I.6.1 The Sun

- The sun is a pseudo-spherical star with a diameter of approximately 1,391,000 km. It is located at an average distance of about 150,000,000 km from Earth. Composed mainly of gaseous matter, primarily hydrogen and helium, it undergoes continuous nuclear fusion reactions, with a core temperature reaching 107 K.[6]
- A black body is an ideal object that would absorb all electromagnetic energy it receives without reflecting or transmitting any. There are no other assumptions about the nature of the object.
- Light, being an electromagnetic radiation, is entirely absorbed, and the illuminated object should appear black, hence the name. However, a black body can emit light if it has a sufficiently high temperature, so it will not appear black under all conditions..

I.6.2 Solar Spectrum

The spectrum of extraterrestrial radiation corresponds approximately to the emission of a black body at 5800 K. A standard curve, compiled from data collected by satellites, is designated as AM 0. Its energy distribution is distributed as follows:

- Ultraviolet (UV): 0.20 <λ< 0.38 μm, 6.4%;
- Visible: 0.38 <λ< 0.78 μm, 48.0%;
- Infrared (IR): 0.78 <λ< 10 μm [7].

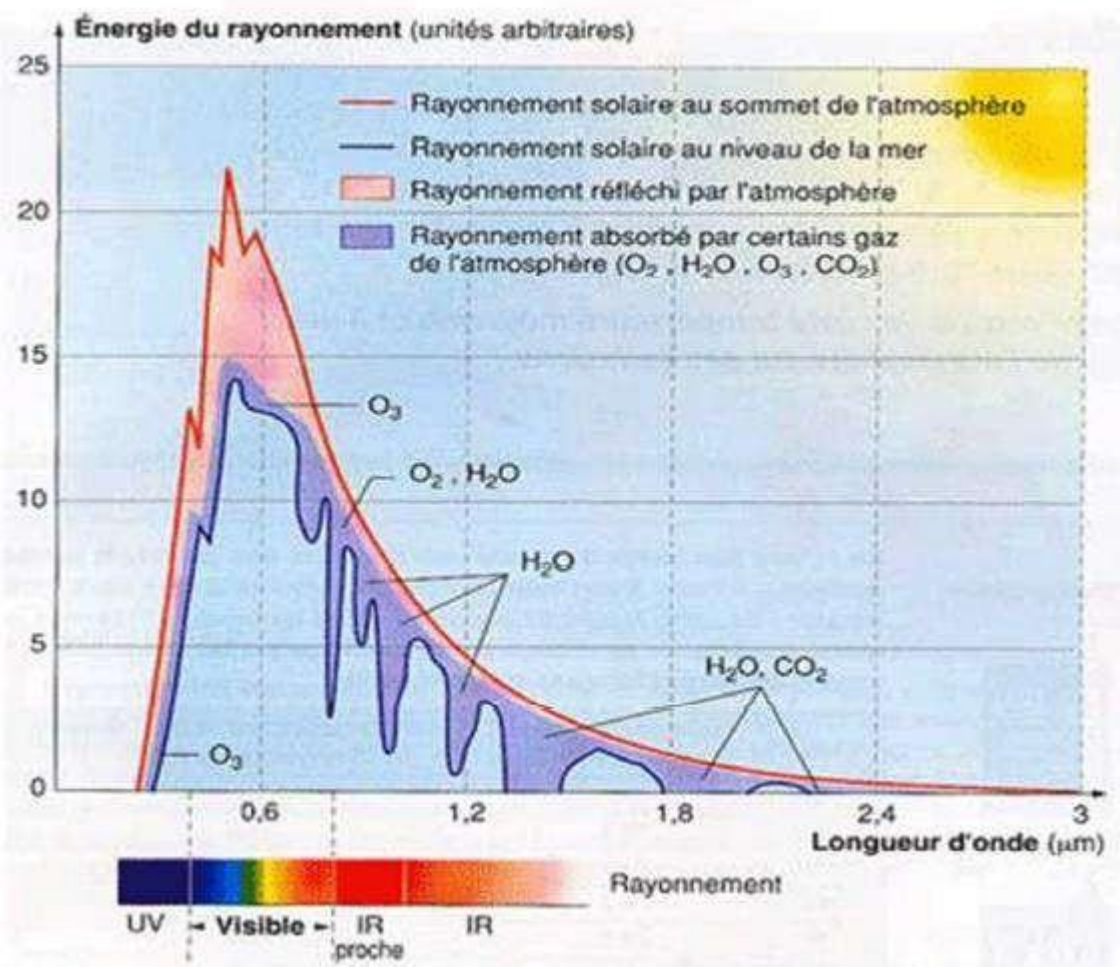

Figure I.4: Solar Radiation Spectrum [8]

However, most of the solar energy is radiated in the ultraviolet, visible, and near-infrared domains: 99.2% of solar energy outside the atmosphere is found between 0.2 μm and 4 μm.

At the ground level, due to the absorption of solar radiation by water vapor, the spectrum is limited to about 2.5 μm (Figure I.4).

At the Earth's surface, the solar spectrum is not the same as in space because it is weighted by the absorption of molecules present in the atmosphere (O3, CO3, H2O,...) [1].

I.6.3 Extraterrestrial Solar Radiation

Solar radiation consists of electromagnetic radiation emitted by the sun, with a spectrum ranging from the smallest wavelengths (gamma rays) to the long radio waves. The parts of this spectrum that play a role in the interaction of solar radiation with the Earth's environment are mainly the infrared, visible, and ultraviolet bands, as well as the radio wave range and the microwave range.

The so-called "extraterrestrial" solar radiation, meaning outside the atmosphere, has been accurately evaluated by NASA and amounts to 1367 W/m². This is the irradiance received, or the instantaneous solar radiation above the Earth's atmosphere, at normal incidence (i.e., on a plane perpendicular to the direction of the sun).

This value is called the "solar constant," but it is not entirely constant due to slight variations in the Earth-Sun distance. When this radiation passes through the atmosphere to reach the Earth's surface, it is greatly attenuated due to absorption and scattering by the various components of the atmosphere.

Solar radiation propagates at the speed of light. Therefore, it takes an average of 499 seconds, or 8 minutes and 19 seconds, to reach our atmosphere [1][9].

I.6.3.1 Solar Radiation Received at the Ground

Solar radiation is the set of electromagnetic waves emitted by the Sun.

a) Components of Solar Radiation

There are four types of radiation:

- Direct Radiation

Direct radiation is the light that reaches the ground directly from the sun on a clear sky.[10]

- Diffuse Radiation

This is due to the absorption and scattering of a portion of the total solar radiation by the atmosphere and its reflection by clouds and aerosols.

- Reflected Radiation or Ground Albedo

This is the radiation that is reflected by the ground or by objects on its surface. Ground albedo can be significant when the ground is particularly reflective (water, snow, etc.).

- Global Radiation

Global radiation is subdivided into direct, diffuse, and ground-reflected radiations.

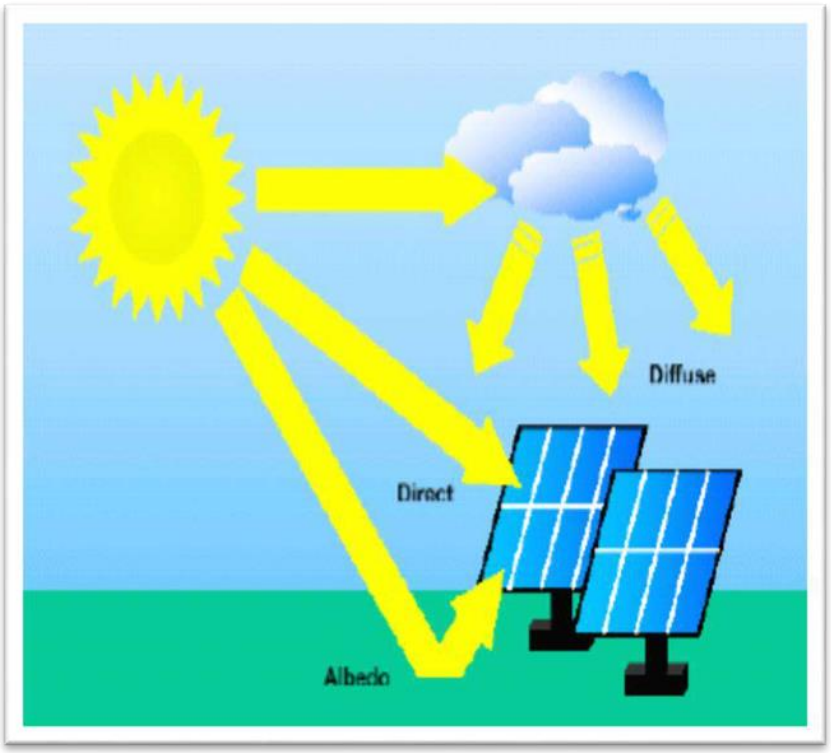

Figure I.5: Components of Solar Radiation Received at the Ground [11].

I.6.4 Solar Potential

I.6.4.1 Solar Potential in Algeria

Solar potential is a set of data describing the evolution of available solar radiation over a given period. It is used to simulate the operation of a solar energy system and to size it as accurately as possible according to the demand to be met.

Due to its geographical location, Algeria has enormous solar potential as shown in Figure (I.6).

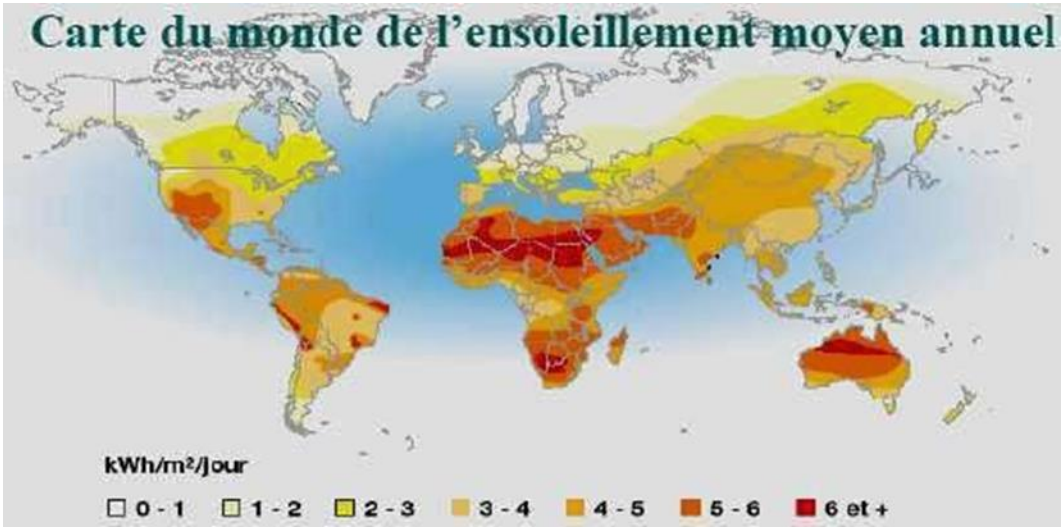

Figure I.6: Map of the World Showing Average Annual Sunshine

Following an evaluation by satellites, the German Aerospace Center (DLR) concluded that Algeria has the highest solar potential in the entire Mediterranean basin, with 169,000 TWh/year for solar thermal energy and 13.9 TWh/year for photovoltaic solar energy.

The distribution of solar potential by climatic region in the Algerian territory is represented in Table I.1 according to the annual received sunlight.

Table I.1: Sunshine Received in Algeria by Climatic Regions1

Regions	Coastal Regions	High Plateaus	Sahara
Area (%)	4	10	86
Average Sunshine Duration (hours/year)	2560	3000	3500
Average Energy Received (kWh/m2/year)	1700	1900	26500

The duration of sunshine in the Algerian Sahara is around 3500 hours/year. It is the highest in the world, always exceeding 8 hours/day and can reach up to 12 hours/day during the summer, except in the extreme south where it decreases to 6 hours/day in the summer

.

The Tamanrasset region is particularly sunny and has the greatest potential in all of Algeria (Figure I.7).

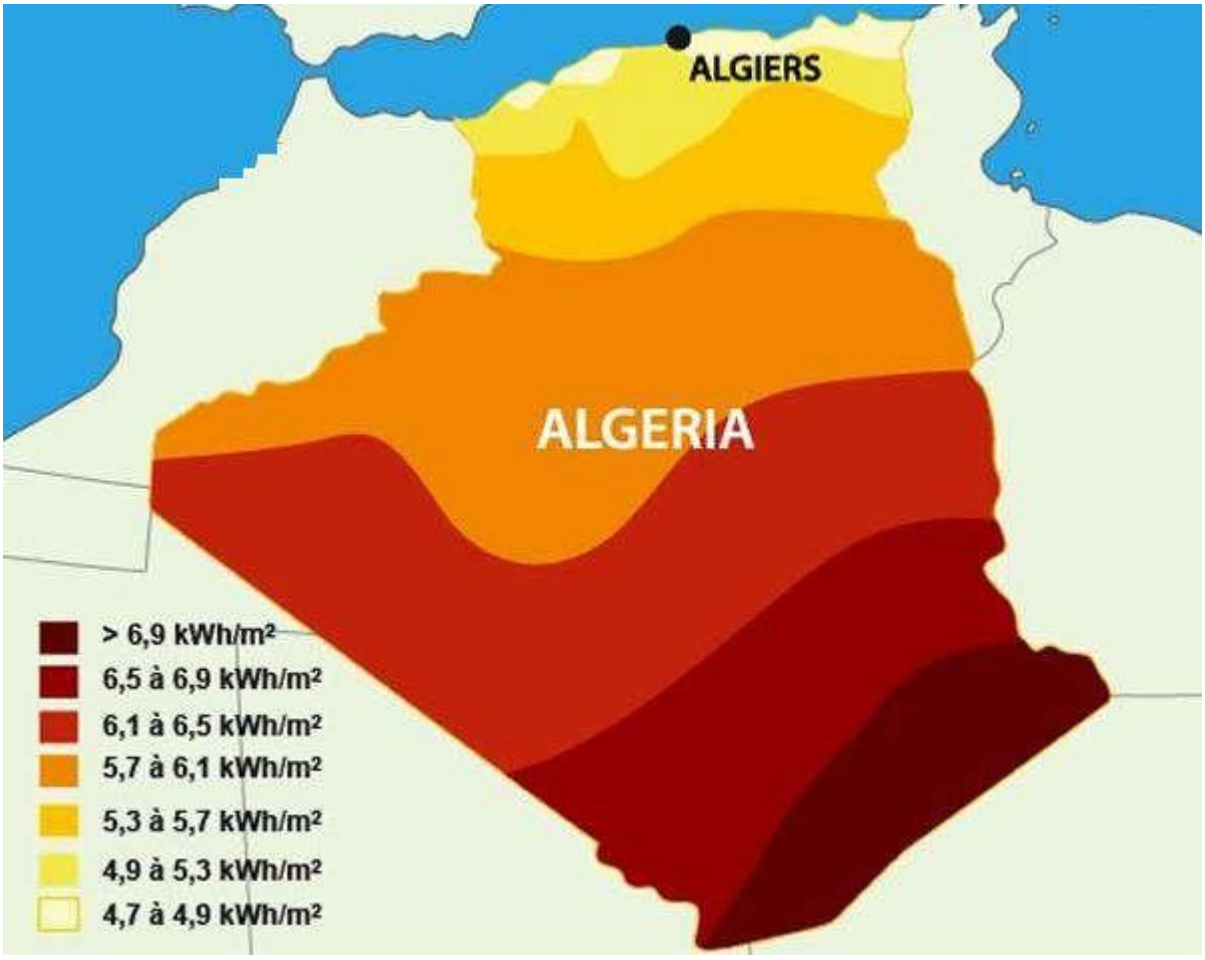

Figure I.7: Annual Average of Global Solar Irradiance Received on an Inclined Plane at the Latitude of the Location

I.7. Overview of Direct Current Machine:

A direct current (DC) motor is a rotating electrical machine that plays a very important role in the industrial field. It is an electromechanical converter that allows bidirectional energy conversion between an electrical system powered by direct current and a mechanical device used to convert electrical energy into mechanical energy – rotation, which is useful energy.

The structure of motors is identical to that of generators, so a DC machine can be used as either a motor or a DC generator. The DC motor is one of the most widely used machines in various sectors. Essentially, this machine is a variable-speed machine. [13]

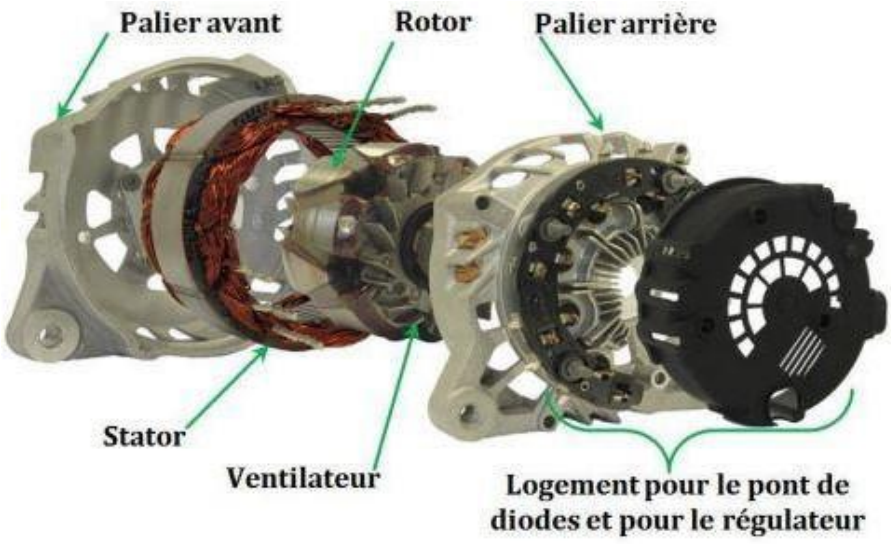

Figure I.8: Diagram of the Construction of a Direct Current Motor

I.7.1 Constitution of the Direct Current Machine

The direct current motor consists of three main parts:

- The armature
- The field winding
- The commutator device

I.7.1.1 The Stator (The Field Winding)

Figure I.9The Stator

This is the fixed part of the motor, composed either of permanent magnets or coils placed around the pole cores (pole cores made of laminated sheets to reduce eddy current losses). When a direct current flows through the coils, it creates a magnetic field in the magnetic circuit of the machine, especially inside the air gap, which separates the fixed part from the moving part.

I.7.1.2 The rotor (the armature)

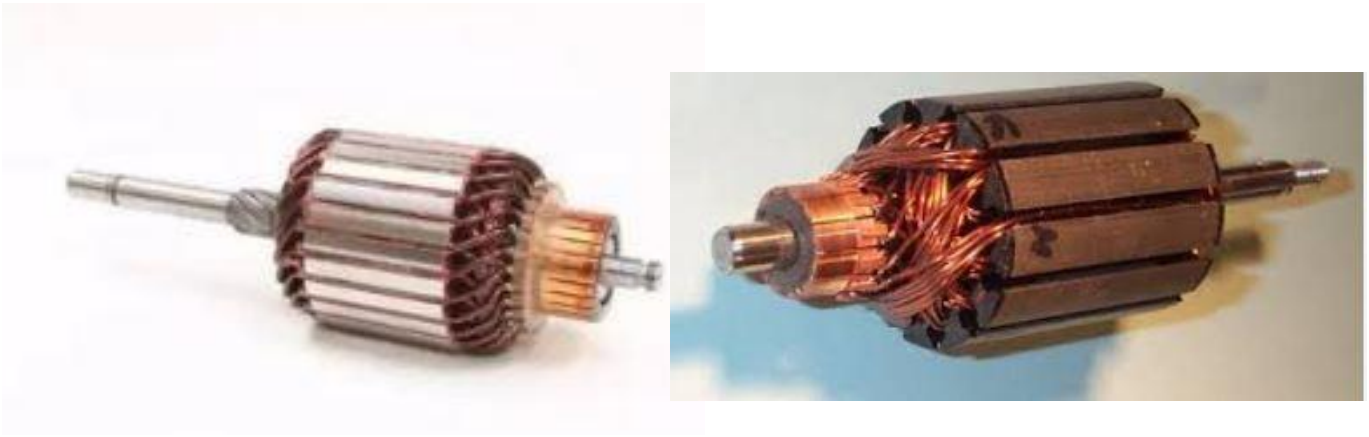

Figure I.10: Rotor

This is the rotating (movable) part of the motor. It carries conductors through which a direct current passes (motor supply); these coils are subjected to forces called "Lorentz forces,"

which rotate the rotor. It is referred to as the armature in terms of the general performance of the machine.

I.7.1.3 Commutator / Brushes

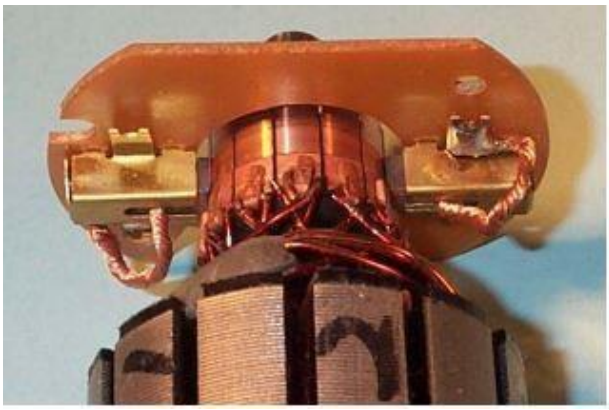

Figure I.11: Commutator/Brushes of the DC Motor

- Commutator: It is a cylindrical assembly of copper fins insulated laterally from each other. These fins are electrically connected to the armature winding, meaning it converts alternating current in the winding into direct current. It is a mechanical switch that reverses the direction of the feeding current in the armature conductors crossing the neutral line.
- Brushes: Made of carbon for its good electrical conductivity and low coefficient of friction, ensuring electrical connection (sliding contact) between the fixed part and the rotating part, hence parallel placement of the brushes is necessary. [13]

I.7.2 Principle of Operation of the Direct Current Machine

The operation of the motor is based on the circulation of a direct current **I** in an excitation winding, which produces a magnetic induction flux **B** in the air gap. If a continuous potential difference is applied between the brushes, the armature conductors located under the same pole (on the same side of the brushes) are traversed by a current of the same direction,

immersed in an inductor induction field. According to the law of Laplace, they are therefore subjected to an electromagnetic force.

$$d\vec{F} = I\vec{d}I \wedge \vec{B} \quad \text{(I.1)}$$

The combination of forces forms a torque whose action tends to rotate the armature [7]

I.7.3 Different Excitation Modes

Direct current motors differ in how they provide excitation energy. The various possible cases are:

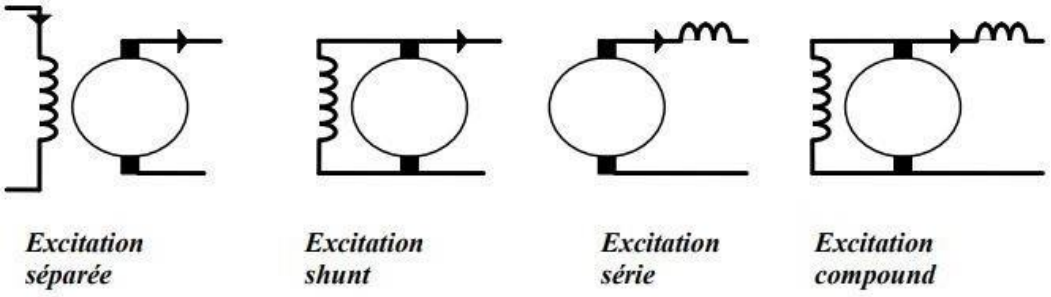

Figure I.12: Diagrams of Different Types of Excitation

I.7.3.1 Separate (Independent) Excitation Motor:

This excitation mode requires two separate power sources. The excitation winding is powered from an independent source of the main supply. The direction of rotation is changed by swapping the terminals of the armature or the field winding.

I.7.3.2 Shunt (Parallel) Excitation Motor:

The excitation winding is connected in parallel with the motor supply and has the same characteristics as the motor with a shunt excitation circuit, since in both cases the induction coil is an external circuit to the motor.

I.7.3.3 Series Excitation Motor:

The field winding is placed in series with the motor armature. Its peculiarity is that it has an inductance through which the same current flows. Therefore, the field has a lower resistance than other types of machines. The inductance is in series with the armature: only one power

supply is required. Reversing the connections of the armature and field changes the direction of rotation.

I.7.3.4 Compound Excitation Motor:

It is a combination of the two previous cases (shunt and series). The first inductance is connected in series with the armature and the second inductance is connected in parallel.

I.7.4 Selection of Direct Current Motor

The selection of a direct current motor should enable driving the machine as well as meeting the performance requirements outlined in the specifications, including:

- Number of operating quadrants;
- Torque over the entire speed range: characteristic $C_r = f(\Omega)$;
- Maximum/minimum speed;
- Maximum acceleration and deceleration

Additionally, adherence to standards for the energy supply network is crucial:

- Reactive energy consumption
- Harmonic distortion imposed on the network
- Electromagnetic compatibility [14]

I.7.5 Advantages and Disadvantages of Direct Current Machines

Direct current (DC) machines offer significant advantages, particularly in the case of motors. They are less polluting and quieter, they start on their own easily, they are easy to use with frequent starts, they offer regularity of usable torque, and they allow for changing the direction of rotation without the intervention of mechanical devices.

However, DC machines also come with disadvantages. These disadvantages include:

- Sensitivity of certain parts, notably the collector and the brushes, considered weak points of DC machines. The brushes must be replaced periodically to ensure optimal contact.

- The price of a DC motor is more than double that of a three-phase asynchronous motor of the same power [15].

I.8. Conclusion

In this chapter, we introduced photovoltaics, semiconductors, and the various types of solar radiation including direct, diffuse, albedo, and global. Additionally, we discussed important concepts related to solar potential in Algeria, such as evaluating expected solar energy and utilizing solar technology for efficient electricity generation in the Algerian environment.

Furthermore, we explored the photovoltaic generator powering the direct current machine controlled by the Maximum Power Point Tracking (MPPT) algorithm for enhanced performance. This aspect focused on controlling the electrical output of solar cells to achieve maximum power generation. We also reviewed the operation of the generator and how its performance is improved through the mentioned algorithm. We will delve deeper into this topic in the next chapter, which will cover simulation and demonstrate the application of the MPPT algorithm to the photovoltaic generator for optimal performance.

Additionally, we examined the direct current machine and its various components, including differences in excitation systems and the electrical and mechanical equations applied to a specific type of excitation. This contributes to a better understanding of the solar power generation process and improves its performance.

Chapter II
Modeling of the Photovoltaic System

II Introduction

The accurate modeling of photovoltaic (PV) systems is crucial for understanding their behavior, optimizing their performance, and designing efficient control strategies. Mathematical models play a vital role in predicting the output characteristics of PV systems under various operating conditions, such as temperature, irradiance levels, and partial shading scenarios.

In this chapter, we delve into the development of mathematical models for the fundamental components of a PV system, including the PV cell, module, and array. These models aim to capture the intrinsic electrical characteristics and the influence of environmental factors on the system's performance.

The modeling process begins with the PV cell, the basic building block of the system. By analyzing the semiconductor principles and the physics of the photovoltaic effect, we derive a mathematical representation of the current-voltage (I-V) relationship for a single PV cell. This model incorporates parameters such as the ideality factor, saturation current, and series and shunt resistances, which account for the non-ideal behavior of the cell.

Subsequently, we extend the cell model to the PV module level, considering the interconnection of multiple cells and the impact of partial shading and temperature variations across the module's surface. The module model is then further expanded to represent the behavior of a complete PV array, which consists of multiple modules connected in series and parallel configurations.

Throughout this chapter, we explore various modeling techniques, ranging from analytical approaches based on semiconductor theory to empirical models derived from experimental data. The strengths and limitations of each modeling approach are discussed, providing insights into their applicability in different scenarios.

Additionally, we examine the influence of environmental factors, such as ambient temperature, wind speed, and solar irradiance, on the performance of the PV system. These factors are incorporated into the models to accurately predict the system's output under real-world operating conditions.

The accurate modeling of PV systems is not only essential for system design and performance evaluation but also plays a crucial role in the development of advanced control strategies, such as maximum power point tracking (MPPT) algorithms and fault detection and diagnosis techniques.

By the end of this chapter, readers will have a comprehensive understanding of the mathematical models governing the behavior of PV systems, enabling them to analyze, optimize, and design efficient and reliable solar energy systems

II.1. Modeling of a Photovoltaic Cell

Studying the characteristics of a photovoltaic cell requires the development of a mathematical model. The cell is typically represented by an equivalent circuit whose parameters are experimentally calculated using the current-voltage characteristic.

Several mathematical models have been developed to represent the nonlinear behavior of the photovoltaic cell, such as the single-diode model (5 parameters) and the two-diode model (8 parameters).

II.1.1 Ideal Model

The photovoltaic cell is represented as an ideal current source that provides a current (photocurrent) proportional to the illumination, shunted with a diode. The equivalent electrical circuit of the photovoltaic cell for the ideal model is depicted in Figure II.1.

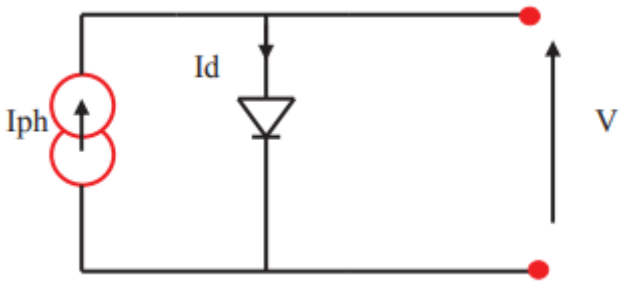

II-1.*Ideal Photovoltaic Cell Model*

From the equivalent circuit, we can write:

$$I = I_{\text{ph}} - I_D \tag{II.1}$$

$$I_D = I_O(e^{\frac{Ve}{nV_T}} - 1) \tag{II.2}$$

$$V_T = \frac{KT}{q} \tag{II.3}$$

• Ie: Current generated by the cell.

• Iph: Photocurrent.

• Id: Current passing through the diode.

• $Isat$: Diode saturation current.

• Ve: Voltage across the cell terminals.

• VT: Thermal voltage.

• K: Boltzmann constant (K = 1.38 × 10^−23 J/K).

• q: Electron charge (q = 1.602 × 10^−19 C).

• T: Cell temperature in Kelvin.

• n: Ideality factor of the junction.

II.1.2 Photovoltaic cell model

An equivalent circuit of a PV cell consist of a current source (I_{ph}), a resistor in series (Rs) and a resistor in parallel (Rp). The resultant current is the difference between the photocurrent I_{ph}, the series resistor current (I) and the parallel resistor current (Ip) as shown in figure 1.6.

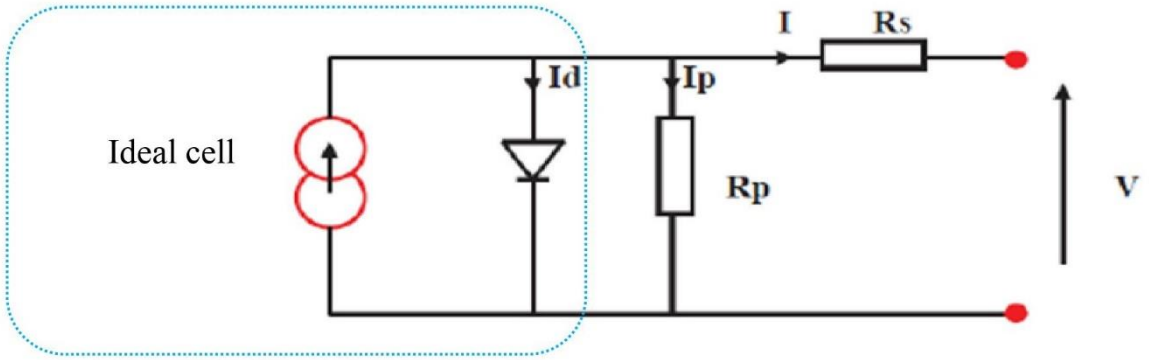

Figure II-2 Equivalent circuit of an ideal photovoltaic cell [17]

By using the Kirchhoff's current law (KCL) and the diode equation that the output current produced by the PV cell is:

Output current $$I = I_{ph} - \left[e^{\frac{q(V+IR_S)}{nKNT}} - 1\right] - I_{sh} \quad (II.4)$$

Where:

I_{ph} is a photo-current :

$$I_{ph} = [I_{sc} + K_i(T - 298)]\frac{G}{1000} \quad (II.5)$$

I_0 is a saturation current :

$$I_0 = I_{rs}[\frac{T}{T_n}]^3 e^{\frac{qEgo(\frac{1}{T_n}-\frac{1}{T})}{nK}} \quad (II.6)$$

I_{rs} is a reverse saturation current

$$I_{rs} = \frac{I_{sc}}{e^{(\frac{qV_{OC}}{nN_SKT})-1}} \quad (II.7)$$

I_{sh} is a current through shunt resistor

$$I_{sh} = (\frac{V+IR_S}{R_{sh}}) \quad (II.8)$$

Where:

I_{ph}	Photo current(A)	I_{sh}
I_{sc}	Short circuit current(A)	I_{sc}
k_i	Short circuit current of cell at 25 °C and 1000 w/m^2	0.0032
T	Operating temperature (K)	T
T_n	Nominal temperature (K)	298
G	Solar irradiance (W/m^2)	G
q	Electron charge (C)	$1.6*10^{-19}$
V_{oc}	Open circuit voltage (V)	V_{oc}
n	The ideality factor of the diode	1.3
K	Boltzmann's constant (J/K)	$1.38*10^{-23}$
E_{g0}	Band gap energy of the semiconductor (eV)	1.1
N_s	Number of PV cells connected in series	Ns
N_p	Number of PV cells connected in parallel	N_p
R_s	Series resistance (Ω)	0.221
R_{sh}	shunt resistance (Ω)	415.405
V_t	Diode thermal voltage (V)	……..

In this project we chose the single diode model as it is simple and easy to implement

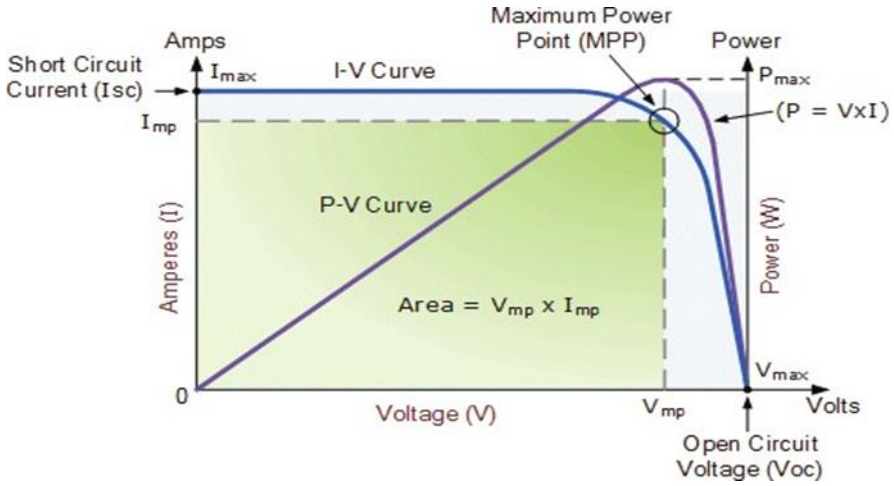

Figure II-3 I-V and P-V characteristics of a photovoltaic module.[18]

The characteristics of a PV module are illustrated in figure II-4 above where: Voc: Open – Circuit Voltage is the maximum voltage that an array produces when the terminals are not connected to any load (an open circuit condition).

Isc: Short-circuit current is the maximum current provided by the PV array when the output connectors are shorted together (a short circuit condition).

MPP: Maximum power point is related to the point where the power supplied by the array that is connected to the load (batteries, inverters) is at its maximum value which is a product of Vmp and Imp.

FF: Fill Factor indicates an important role when comparing the performance of different photovoltaic module. A high fill factor is equal to a high-quality module which has low internal losses.

II.2. Arrangement of photovoltaic cells

Photovoltaic (PV) generators are made of multiple interconnected PV cells linked together to form a PV module. When multiple modules are interconnected together, they form a PV array. The connection of these PV modules can either be, series, parallel or both, and the type of connection depends on the voltage and the current levels desired by the power processing system dedicated to the PV generator.

II.2.1 String connection of photovoltaic cells

The photovoltaic cells are arranged in series in photovoltaic panels. This type of configuration is applied because the operating voltage is few hundreds of millivolts as shown in figure II.4:

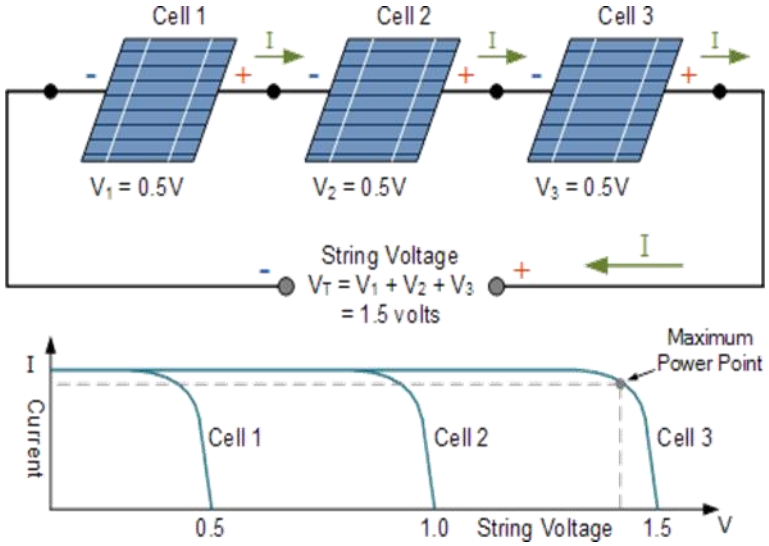

Figure II-5 . Series connection of solar cells [19]

So, the PV cells are connected in series to form strings in order to reach a voltage level that meets the input requirements of the power processing system

II.2.2 Parallel arrangement of photovoltaic cells.

The figure 1.9 illustrated how the generated current can be increase through parallel connection of photovoltaic cells:

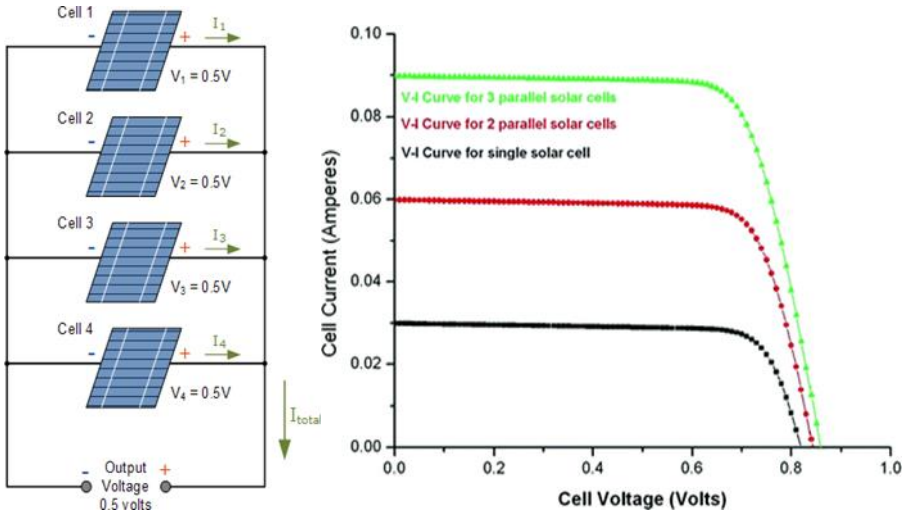

II-6 Parallel connection of photovoltaic cells [19]

Therefore, a parallel arrangement of photovoltaic cells increases the output current as The potential difference across the terminals is constant

II.2.3 Parallel and series connection of photovoltaic cells

The parallel and series connection of PV cells increases the output voltage and current. The output voltage is obtained by multiplying the voltage value of each cell by the number of cells in series of each panel. The resultant output current is obtained by multiplying the cell current values by the number of strings connected in parallel.

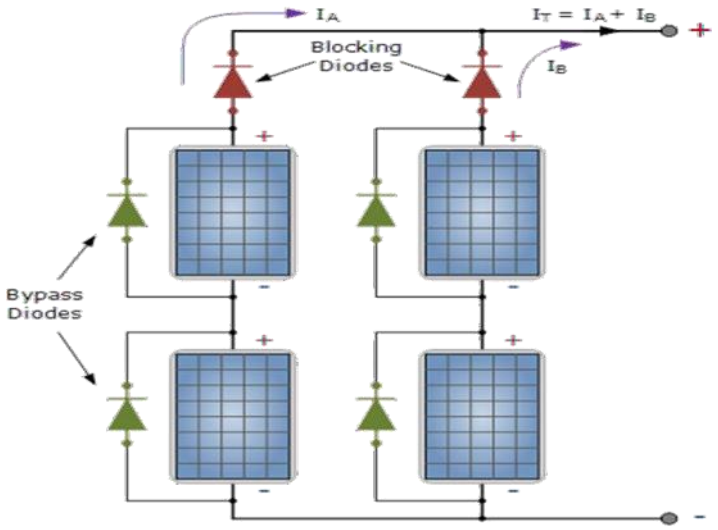

Figure II-7 Parallel and series connection of photovoltaic cells [20]

In the event of an accident where one cell is broken or simply disconnected, the current of all the cells in series in the string is interrupted and the power contribution of the whole string is missed. The effect of such events is solved by PV panel manufacturers, whereby, they connect a bypass diode in parallel to the PV cell, usually two or three depending on the power rating of the PV panels

II.3. Effect of temperature and irradiance on the performance of a PV module

In order to determine using MATLAB/Simulink the effects of temperature and irradiation on the performance of a PV panel, a SUNTECH POWER STP250S -20-Wd solar panel integrated in MATLAB library has been chosen with the following parameters: Table II.1. Electrical Characteristics of the module (STC, 1000W/m2, 25°C, AM = 1.5)

Parameters (STC)	Values
Rated power (Vmp)	200.22
Voltage at maximum power (Vmp)	47
Current at maximum power (Imp)	4.26
Open circuit voltage (Voc)	57.6
Short circuit current (Isc)	4.6
Total number of cells in series (Ns)	2
Total number of cells in parallel (Np)	1

II.3.1 Effect of temperature on the performance of a PV module

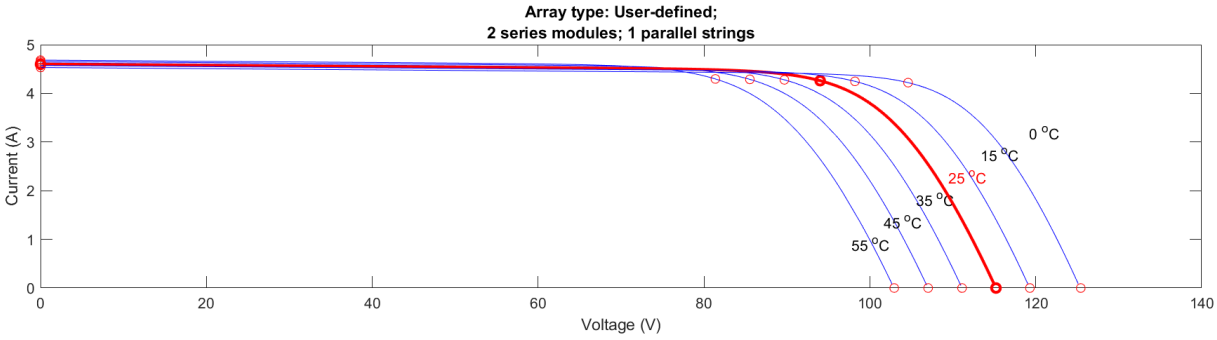

Figure II-8 Effect of temperature on output voltage and current

When the irradiance is maintained at 1000W/m2, the voltage and current of the PV panel is inversely proportional to the temperature as shown in figure II-9

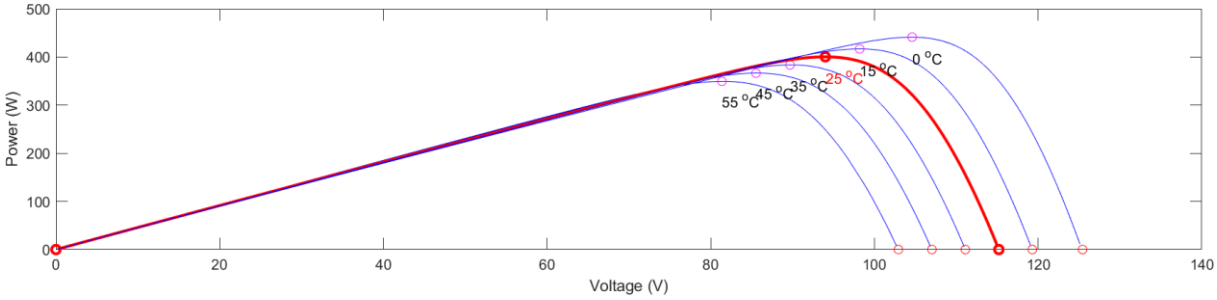

Figure II-10 Effect of temperature on solar power output

The power produced by the photovoltaic modules decreases with an increase in temperature because; the band gap energy decreases and more photons have enough energy to create electron-hole pairs which eventually reduces the efficiency of the panel [21].

II.3.2 Effect of irradiance on the performance of a photovoltaic module

While the temperature is maintained at 25°C, the voltage and current output of a photovoltaic module is directly proportional to the solar radiation as shown in figure II-9

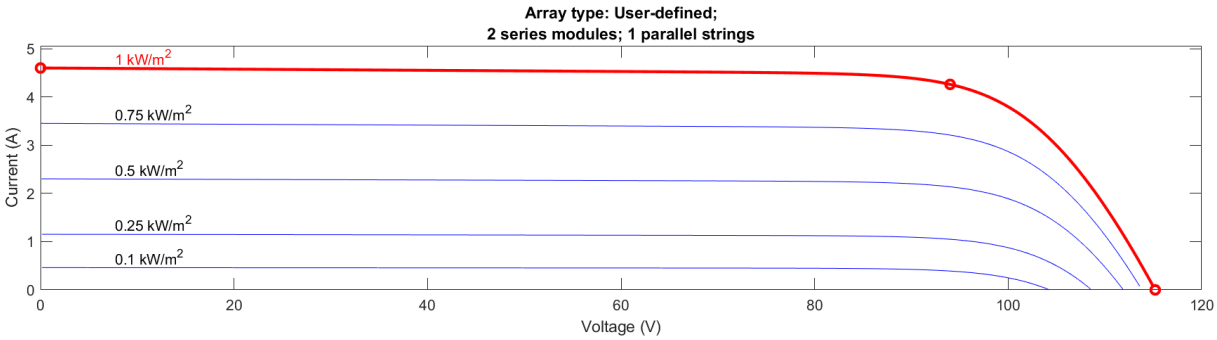

Figure II-11 Effect of the irradiation on the PV voltage and current output

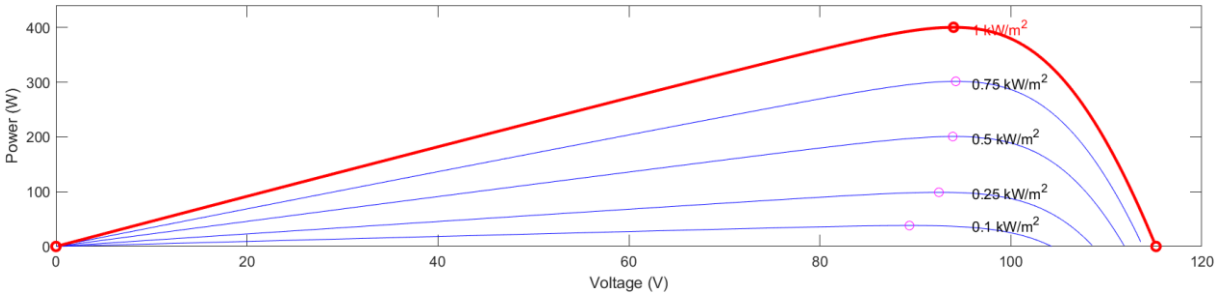

II-12 Effect of irradiation on PV power output

The curves shown in figure II-10 shows that, the power produced by the solar panel is directly proportion to the solar radiation.

Using equations (II.4), (II.5), (II.6), (II.7), and (II.8), we can construct the block diagram for Comprehensive Simulation of the Solar Cell,Irs,Io,Iph,Ish,I :

Comprehensive Simulation of the Solar Cell:

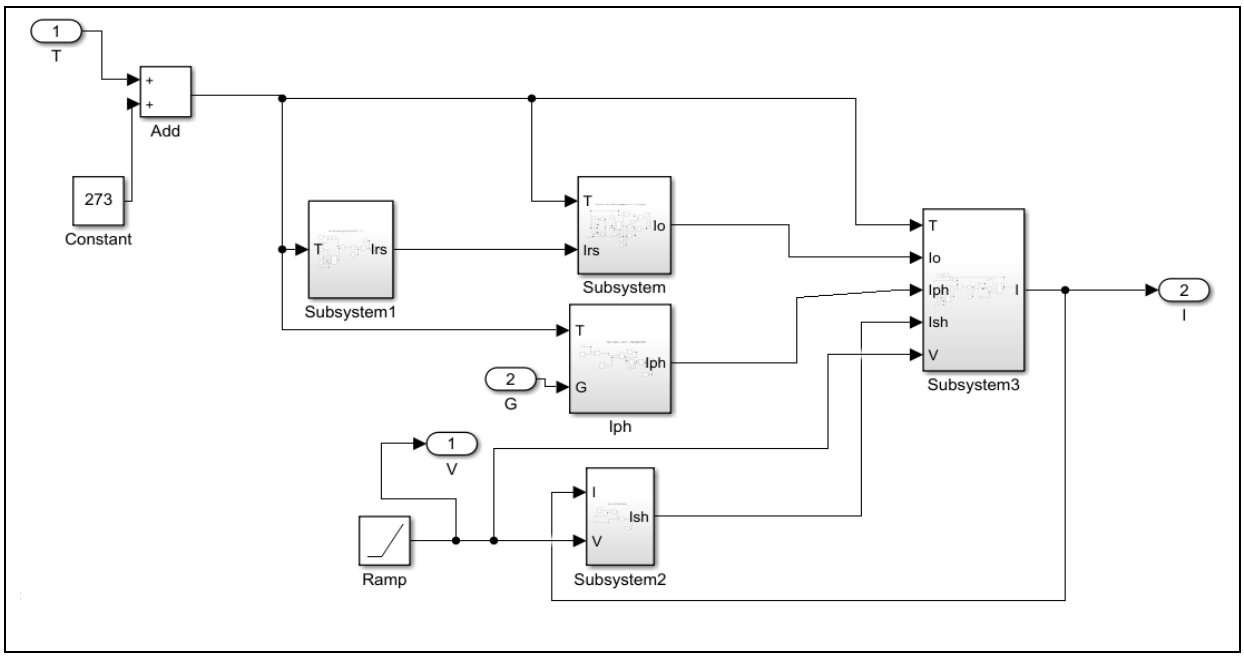

The I_{rs} current:

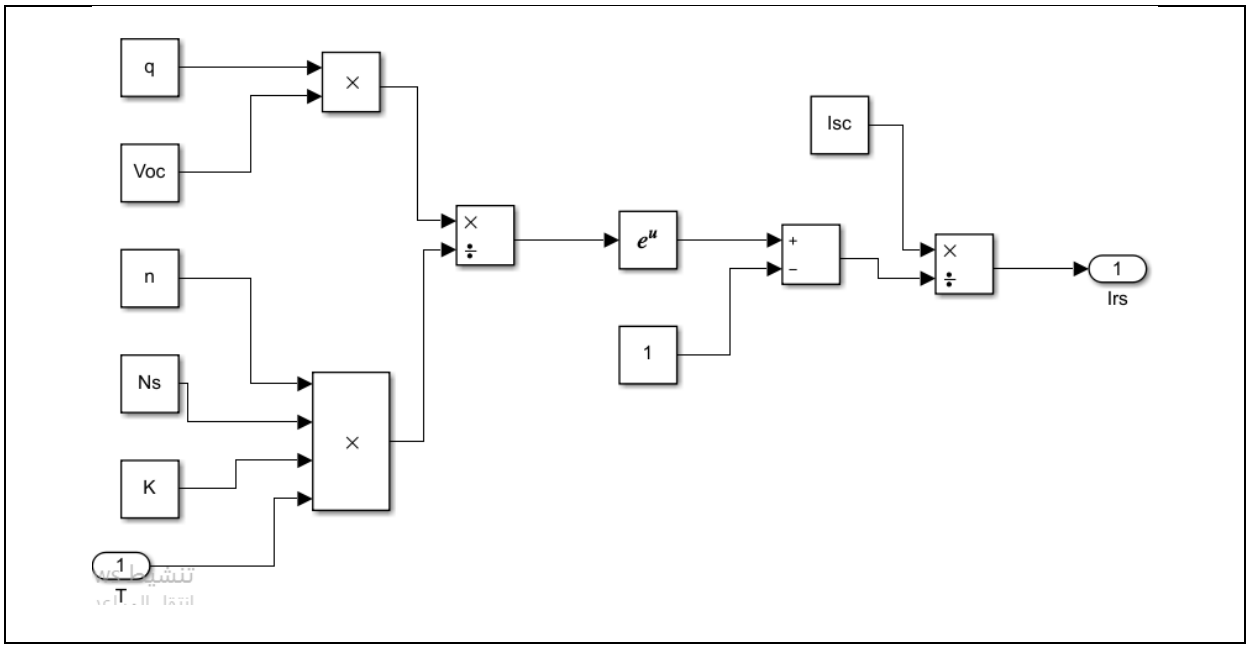

The I_O current:

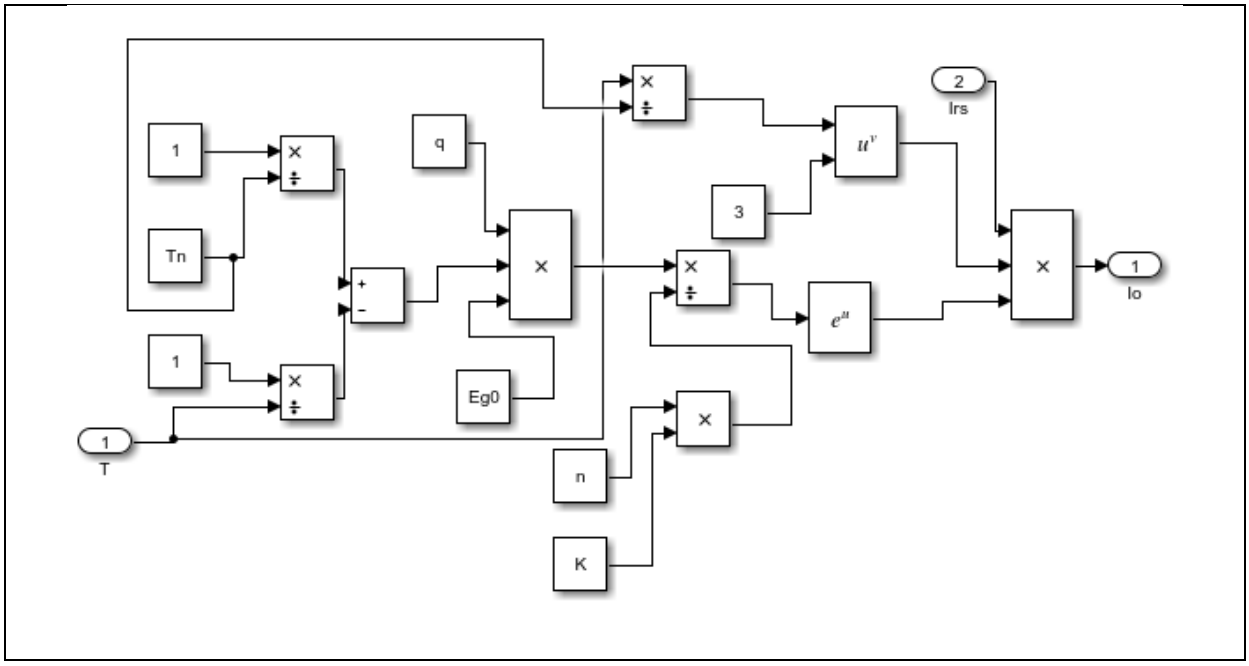

The I_{ph} current:

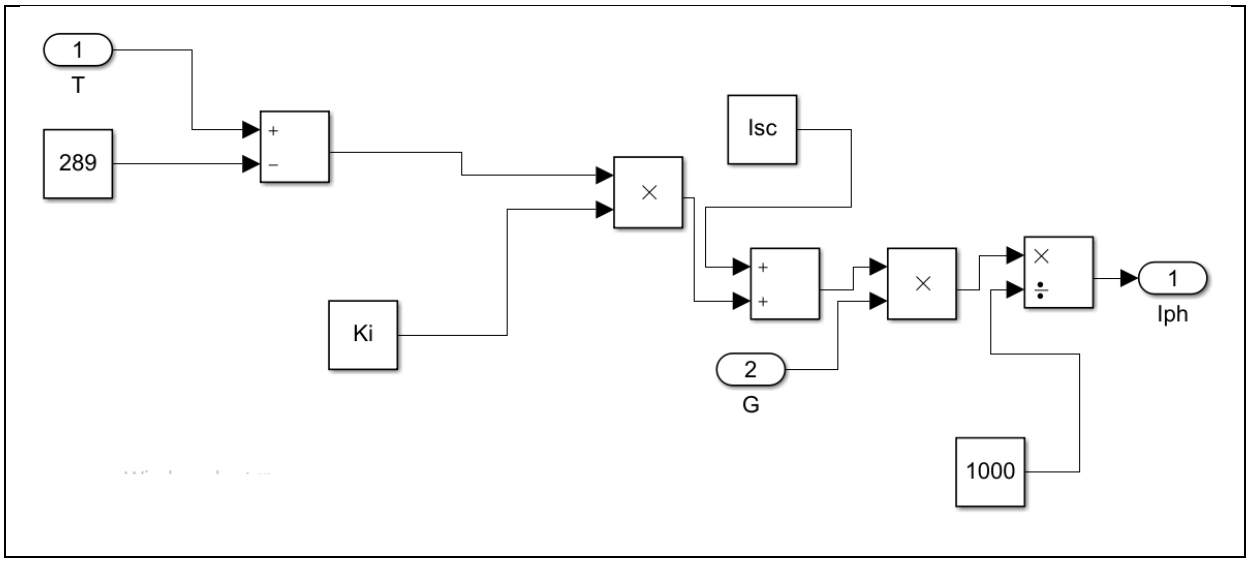

The I_{Sh} current:

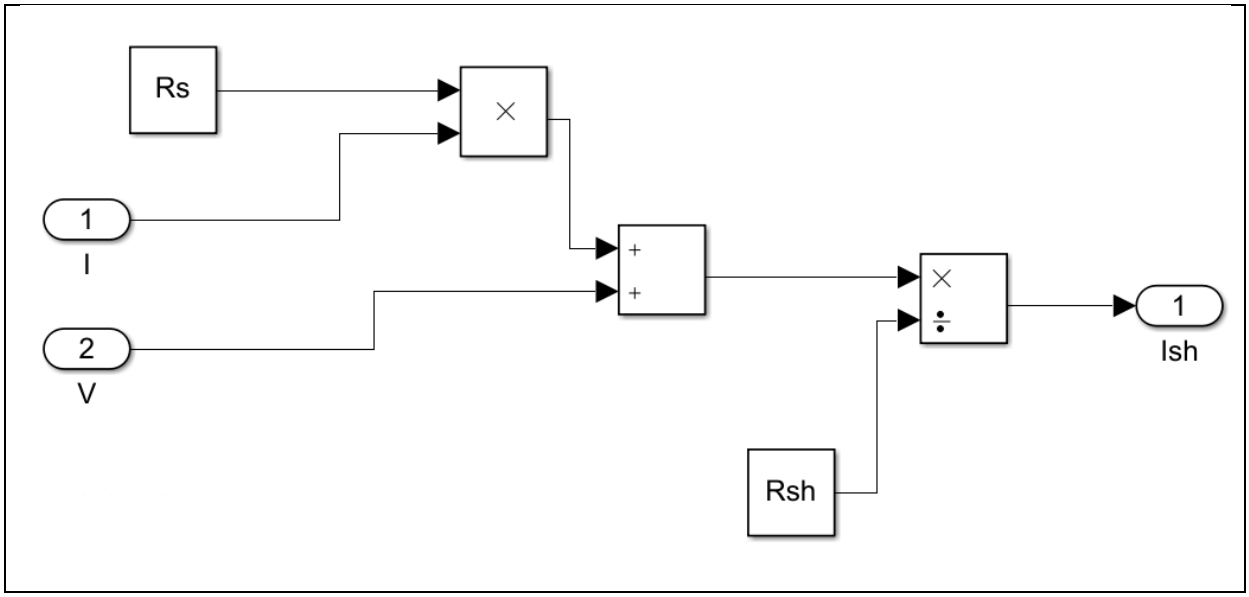

The I current:

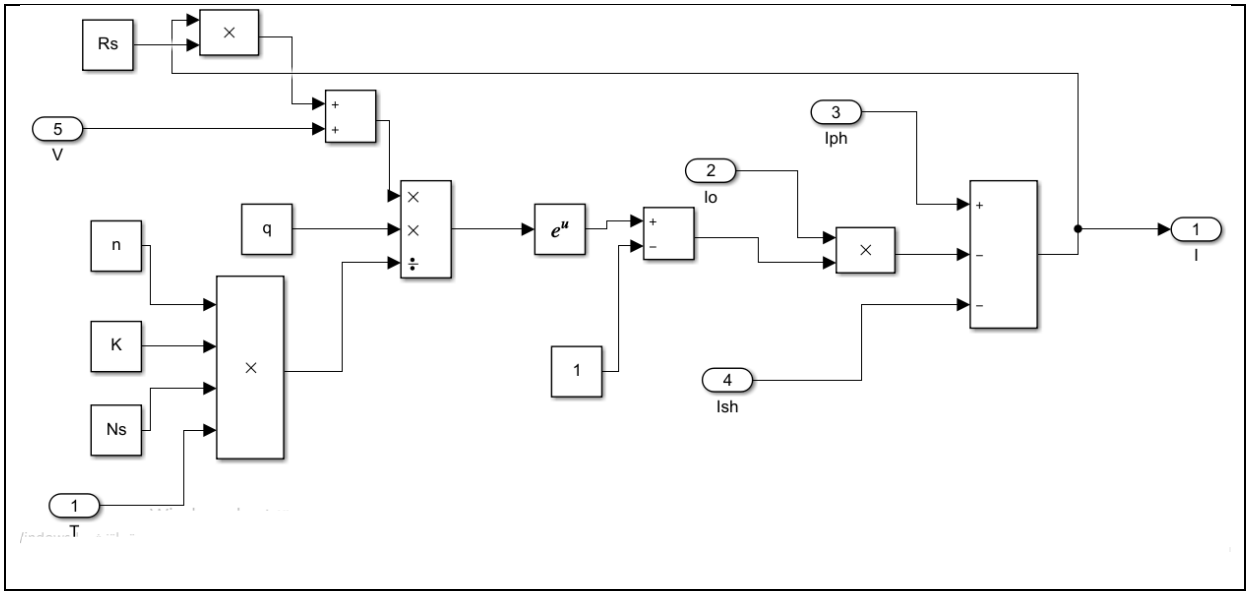

Chapter III
Analysis and Design of Maximum Power Point Tracking (MPPT) Algorithm

III Introduction

A photovoltaic system is mainly composed of a PV generator connected to a load. This connection can be made either directly or indirectly through an adaptation stage. The role of the adaptation stage is to ensure the transfer of maximum power provided by the PV generator to the load using a control system designed for this purpose. When the load is supplied with direct current, the adaptation stage is a DC-DC converter, and the control used is MPPT (Maximum Power Point Tracking). Conversely, for an alternating current load, the adaptation stage represents a DC-AC converter (or inverter) equipped with PWM (Pulse Width Modulation) control.

In this chapter, we will begin by presenting the direct PV-load connection. Then, we will introduce the PV-load connection via a DC-DC adaptation stage. Next, we will define the MPPT control problem and discuss the methods used to address it. Perturbation and observation algorithms and inductance incrementation will be studied subsequently. Simulations will be conducted to illustrate the points discussed in this chapter. Finally, we will conclude the chapter.

III.1. Direct Connection

In the case of standalone installations, PV systems operate independently of the electrical grids. The energy produced by the PV solar panels is either used immediately (for water pumping, ventilation, etc.) or stored in batteries for later use. The direct current produced powers devices directly or is converted into 230 V alternating current via an inverter [2]. The simplest configuration of this connection involves directly connecting the generator and the load with wires. To ensure the flow of current in one direction, i.e., from the generator to the load, a blocking diode is placed between them. This diode can protect the generator in case of a load represented by a battery (in this scenario, the battery might discharge into the generator and damage it).

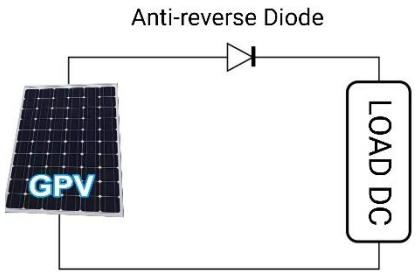

Figure III-1.Direct Connection

The drawback of this configuration lies in the inability to control the system to extract maximum power. Figure II.3 depicts three types of loads that can be directly connected to a PV generator:

- A load of constant voltage source type,
- A load of constant current source type,
- A purely resistive load.

For operating points A, B, and C, the power supplied by the generator is respectively PA, PB, and PC, each of which is lower than the maximum power. The difference in power will therefore be lost and dissipated within the generator in the form of heat.

III.1.1 Direct Connection Simulation

To illustrate the drawbacks of direct connection, we directly connect the PV generator with a resistive load of 15Ω. The temperature is considered constant (T = 25°C), while the illumination varies, as shown in Figure III.2.

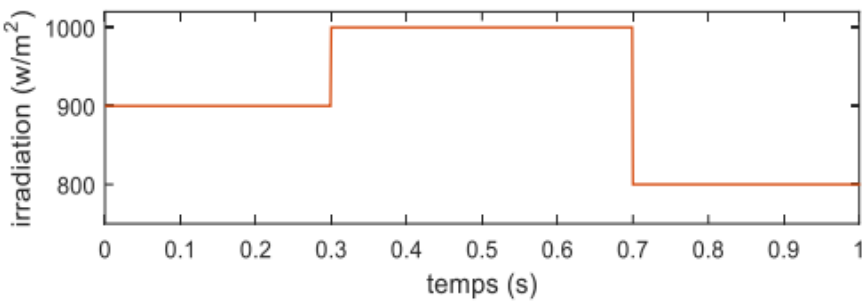

Figure III-2 Irradiation Profile

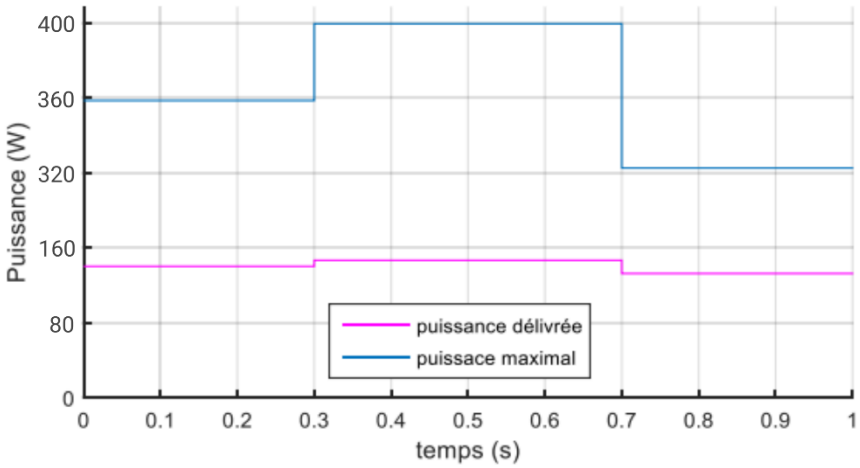

Figure III-3 Operation of GPV in Direct Source/Load Connection.

Discussion

Based on Figure III.3, it is evident that the power delivered by the PV generator is significantly lower than the maximum power it can provide for each irradiance value. The simulation results confirm that the PV generator operates far from the optimal operating point.

III.2. Connection via an Adaptation Stage

The nonlinear characteristics of the PV generator, influenced by temperature and irradiance, result in the nominal power value delivered by the PV generator being significantly different from its maximum value. Indeed, the PV generator has only one optimal operating point (Vppm, Ippm) where the system is intended to operate.

Efficient utilization of solar resources necessitates the use of an adaptation stage, as depicted in Figure III.4. This stage is often a DC-DC converter (chopper), which adjusts the voltage across the PV generator terminals through a control system continuously to extract the maximum power.

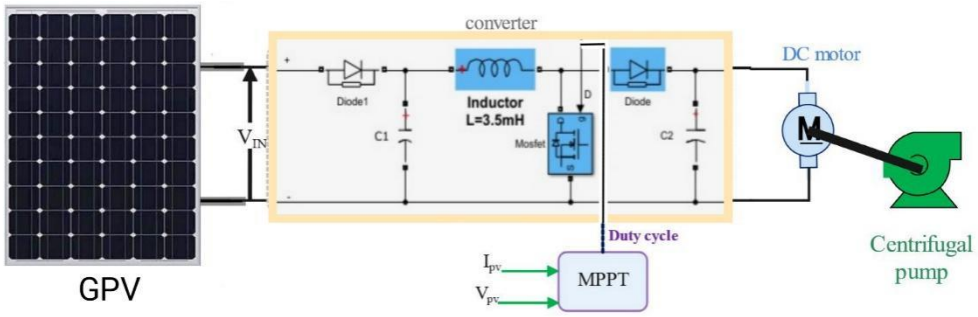

Figure III-4 Connection through an Adaptation Stage

III.2.1 PWM Control

The MOSFET switch is controlled by the pulse width modulation (PWM) technique. The PWM control signal u is generated by comparing the duty cycle $\boldsymbol{\alpha}$ with a triangular signal $Stri$ of amplitude 1 and period $\boldsymbol{T}$. The expression for the control signal is given by equation (III.1).

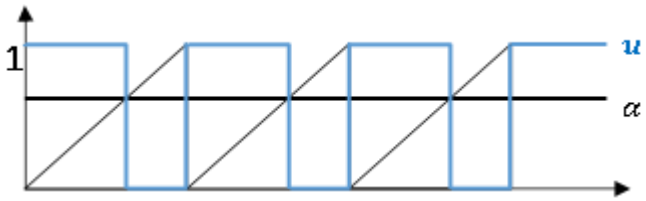

Figure III-5 Signal Generated by the PWM Technique.

$$u = \begin{cases} 1 \ si \ \alpha > T_r \\ 0 \ si \ \alpha < T_r \end{cases} \quad \text{(III.1)}$$

III.3. Power electronic converters

Power electronic devices plays a major in the functioning of photovoltaic system either in stepping up or stepping down DC the voltage generated by the solar panels and these are known as DC-DC converters or during the conversion of direct current to alternating current and these referred to as (DC-AC converters). The choice of these power electronic devices rests entirely on the types of load used, either AC or DC loads

III.3.1 DC-DC converters

These are solid-state power electronic devices that either increase or decrease DC voltage. DC-DC converters operate using Pulse Width Modulation (PWM), where a high-frequency pulse signal is employed to switch the electronic components on and off, thereby regulating the output voltage. These DC-DC converters include:

✓ Buck converters,

✓ Boost converters

✓ Buck – boost converters

III.3.1.1 Buck Converter

The Buck converter, also known as a series chopper, allows the conversion of a DC voltage to a lower DC voltage. Its electrical schematic is shown in Figure III.5.

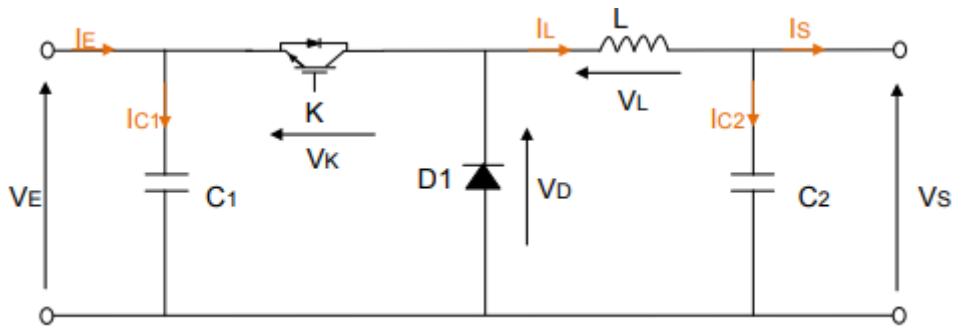

Figure III-6 *Schematic of a Buck Converter*

Note: To ensure current continuity and prevent pulsed currents from affecting the PV generator, it is necessary to place a filter capacitor $\mathbf{C_1}$ (see Figure III.7) between the generator and the converter.

III.3.1.1.1 Operating Sequences

❖ **First Sequence [0 → αT_o]**

The switch is closed for the duration $\boldsymbol{\alpha T_d}$ of the switching period $\mathbf{T_d}$ .During this time, the source voltage $\mathbf{V_e}$ supplies energy to the load through the inductor.

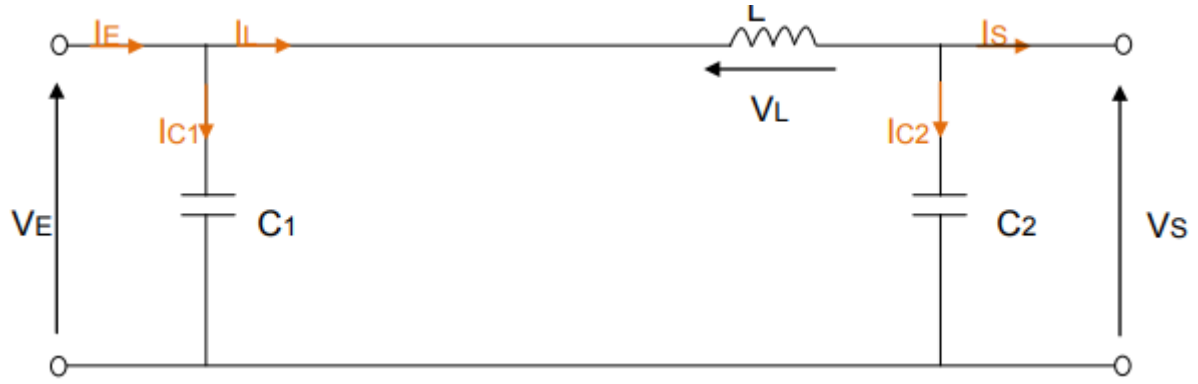

Figure III-7 Equivalent Circuit When the Switch is Closed

By applying Kirchhoff's laws (KVL - Kirchhoff's Voltage Law and KCL - Kirchhoff's Current Law), we obtain the following equations:

$$C1\frac{dV_E}{d_t} = I_E - I_L \Rightarrow \dot{V_E} = \frac{1}{C1}(I_E - I_L) \quad \text{(III.2)}$$

$$L\frac{dI_L}{d_t} = V_E - V_S \Rightarrow \dot{I_L} = \frac{1}{L}(V_E - V_S) \quad \text{(III.3)}$$

$$C2\frac{dV_E}{d_t} = I_L - \frac{V_S}{R} \Rightarrow \dot{V_S} = \frac{1}{C2}I_L - \frac{1}{RC2}V_S \quad \text{(III.4)}$$

❖ **Second Sequence [$\alpha T_d \rightarrow T_d$]**

During this sequence, the switch opens, and the energy stored in the inductor is discharged into the load and the capacitor. The diode ensures the continuity of the current in the inductor.

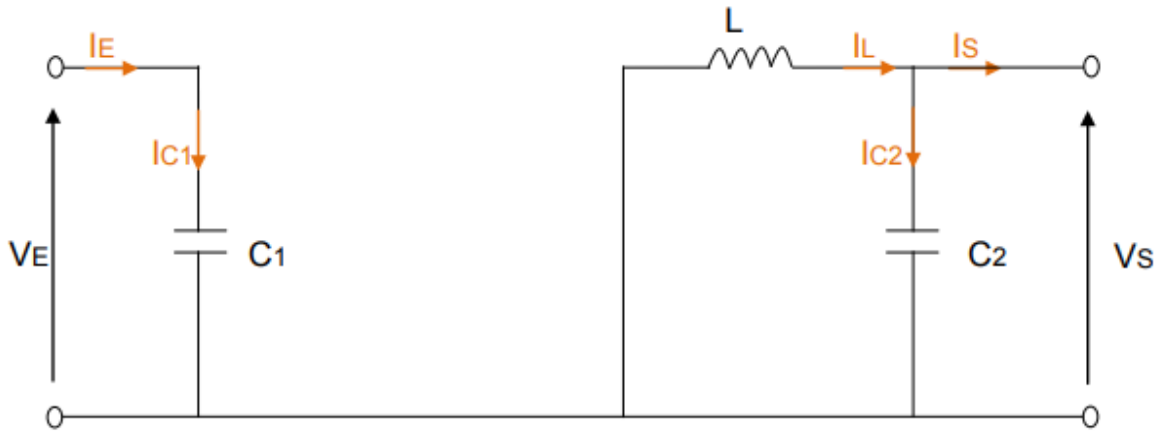

Figure III-8 Equivalent Circuit When the Switch is Open.

By applying Kirchhoff's laws (KVL - Kirchhoff's Voltage Law and KCL - Kirchhoff's Current Law), we obtain the following equations:

$$C1\frac{dV_E}{d_t} = I_E \Rightarrow \dot{V_E} = \frac{1}{C1} I_L \quad \text{(III.5)}$$

$$L\frac{dI_L}{d_t} = -V_S \Rightarrow \dot{I_L} = \frac{1}{L} V_S \quad \text{(III.6)}$$

$$C2\frac{dV_E}{d_t} = I_L - \frac{V_S}{R} \Rightarrow \dot{V_S} = \frac{1}{C2} I_L - \frac{1}{RC2} V_S \quad \text{(III.7)}$$

III.3.1.1.2 Average Model

The average value $\mathbf{E_m}$ of a parameter in the state $\mathbf{E_1}$ closed and the state $\mathbf{E_2}$ open, is given by the following expression:

$$E_m = \alpha E_1 + (1-\alpha) E_2 \quad \text{(III.8)}$$

Applying this expression to the equations of the Buck converter, we find the average model:

$$\dot{V_e} = \frac{1}{C1} I_E - \frac{\alpha}{C1} I_L \quad \text{(III.9)}$$

$$\dot{I_L} = \frac{\alpha}{L} V_E - \frac{1}{L} V_S \quad \text{(III. 10)}$$

$$V_S = \frac{1}{C2} \dot{I_L} - \frac{1}{RC2} V_S \quad \text{(III.11)}$$

III.3.1.1.3 Duty Cycle

In continuous conduction mode, the current through the inductor never becomes zero.

$$V_L = L\frac{dI_L}{dt} \quad \text{(III.12)}$$

During the conduction state: $V_L = V_E - V_S$, the evolution of the inductor current in the circuit is given by:

$$\Delta I_{Lon} = \int_0^{\alpha T} \frac{V_L}{L} = \frac{(V_E - V_S)\alpha T}{L} \quad \text{(III.13)}$$

During the blocking state: $V_L = -V_S$, the evolution of the inductor current in the circuit is given by:

$$\Delta I_{Loff} = \int_{\alpha T}^{T} \frac{V_L}{L} = -\frac{V_S(T-\alpha T)}{L} \quad \text{(III.14)}$$

In steady state:

$$\Delta I_{Lon} + \Delta I_{Loff} = 0 \quad \text{(III.15)}$$

$$\frac{(V_E - V_S)\alpha T}{L} - \frac{V_S(T-\alpha T)}{L} = 0 \Rightarrow V_s = \alpha V_E \quad \text{(III.16)}$$

With $0 \leq \alpha \ll 1$,the output voltage is always less than or equal to the input voltage.

III.3.1.2 Boost converter

Generally, a boost converter as shown in Figure III-9 is a DC-DC converter with an output voltage greater than the source voltage. It is sometimes called a step-up converter since it "steps up" the source voltage as it is designed to provide an efficient method of taking a given DC voltage supply and boost it to a desired value

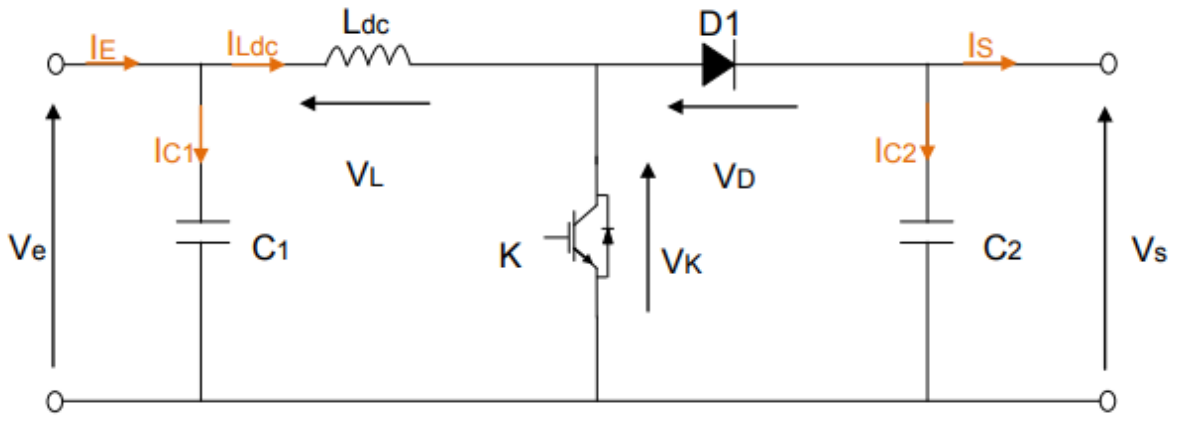

Figure III-9 Schéma d'un convertisseur Boost.

III.3.1.2.1 Operating Sequences

- **First Sequence [0 → αT₀]**

During the duration 0 - αT_d, the switch is closed. The current in the inductor increases gradually, and energy is stored in the form of magnetic energy.

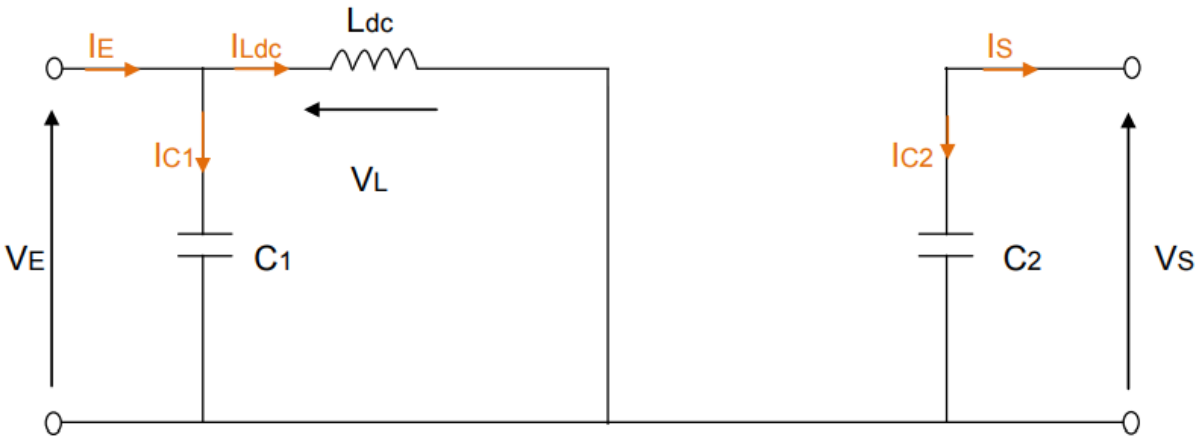

Figure III-10 Equivalent Circuit When the Switch is Closed.

Applying Kirchhoff's laws gives the following equations:

$$C1\frac{dV_E}{d_t} = I_E - I_L \Rightarrow \dot{V_E} = \frac{1}{C1}(I_E - I_L) \quad \text{(III.17)}$$

$$L\frac{dI_L}{d_t} = V_E \Rightarrow \dot{I_L} = \frac{1}{L}(V_E) \quad \text{(III.18)}$$

$$C2\frac{dV_E}{d_t} = -\frac{V_S}{R} \Rightarrow \dot{V_S} = -\frac{1}{RC2}V_S \quad \text{(III.19)}$$

❖ **Second Sequence [$\alpha T_o \rightarrow T_o$]**

During this sequence, the switch opens, and the energy stored in the inductor is discharged into the load and the capacitor. The diode ensures the continuity of the current in the inductor.

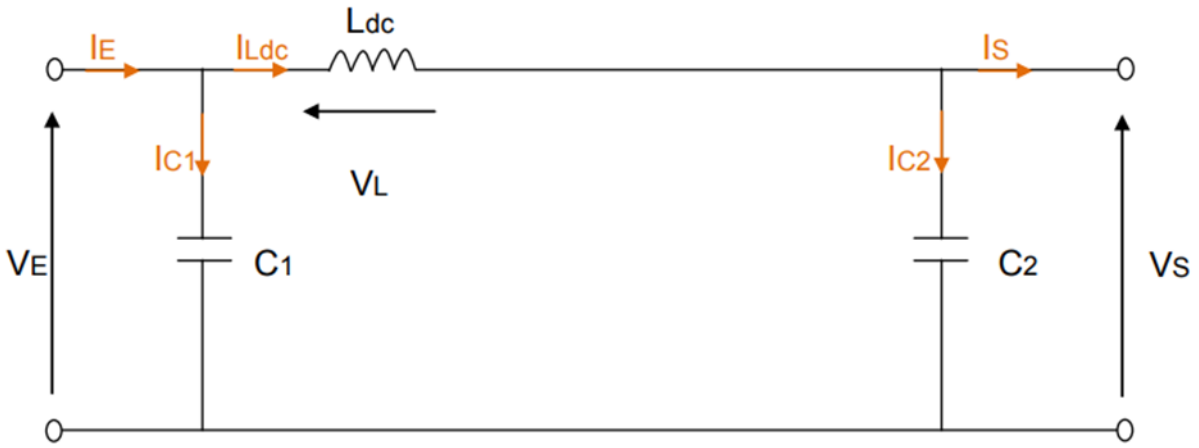

Figure III-11 Equivalent Circuit When the Switch is Open.

Applying Kirchhoff's laws gives the following equations:

$$C1\frac{dV_E}{d_t} = I_E - I_L \Rightarrow \dot{V_E} = \frac{1}{C1}(I_E - I_L) \quad \text{(III.20)}$$

$$L\frac{dI_L}{d_t} = V_E \Rightarrow \dot{I_L} = \frac{1}{L}(V_E - V_S) \quad \text{(III.21)}$$

$$C2\frac{dV_E}{d_t} = I_L - \frac{V_S}{R} \Rightarrow \dot{V_S} = \frac{1}{C2}I_L - \frac{1}{RC2}V_S \quad \text{(III.22)}$$

III.3.1.2.2 Average Model

Applying Kirchhoff's laws gives the following equations:

$$\dot{V_e} = \frac{1}{C1}I_E - \frac{1}{C1}I_L \quad \text{(III.23)}$$

$$\dot{I_L} = \frac{1}{L}V_E - \frac{1-\alpha}{L}V_S \quad \text{(III.24)}$$

$$V_S = \frac{1-\dot{\alpha}}{C2}I_L - \frac{1}{RC2}V_S \quad \text{(III.25)}$$

III.3.1.2.3 Duty Cycle

In continuous conduction mode:

$$V_L = L\frac{dI_L}{dt} \quad \text{(III. 26)}$$

In the conduction state, $V_L = V_e$,the evolution of the inductor current in the circuit is given by:

$$\Delta I_{Lon} = \int_0^{\alpha T} \frac{V_L}{L} dt = \frac{(V_E.\alpha T)}{L} \quad \text{(III.27)}$$

In the blocking state, $V_L = L\frac{dI_L}{dt}$=V_E-V_S, the evolution of the inductor current in the circuit is given by:

$$\Delta I_{Loff} = \int_{\alpha T}^{T} \frac{V_L}{L} dt = \int_{\alpha T}^{T} \frac{(V_E - V_S)}{L} dt = \frac{(V_E - V_S)(1-\alpha)T}{L} \quad \text{(III.28)}$$

In steady state:

$$\Delta I_{Lon} + \Delta I_{Loff} = 0 \quad \text{(III.29)}$$

$$\frac{V_E.\alpha T}{L} + \frac{(V_E - V_S)(1-\alpha)T}{L} = 0 \quad \text{(III.30)}$$

$$V_E = (1-\alpha)V_S \Rightarrow V_S = \frac{1}{1-\alpha} V_E \quad \text{(III.31)}$$

With $0 \leq \alpha \leq 1$ the output voltage is always greater than or equal to the input voltage.

III.4. MPPT Control

In an electrical system comprising a source and a load, finding the optimal operating point using optimization techniques is crucial. In the case of photovoltaic systems, the optimal operating point allows the PV generator to deliver its maximum power, which is highly dependent on factors such as sunlight and ambient temperature. To ensure maximum power operation despite variations in sunlight and temperature, the principle of Maximum Power Point Tracking (MPPT) control is introduced. Various methods have been developed in recent years to implement MPPT control, which can be classified into two variants: direct and indirect methods.

III.4.1 Indirect Methods (Offline Methods)

Indirect methods are based on the knowledge of the nonlinear characteristics of the photovoltaic generator, which is not precisely available. These methods also require the measurement of sunlight and the temperature of the photovoltaic generator. Then, the power curve is consulted to determine the optimal operating current (or voltage). The measured current (or voltage) from the generator is then compared to the optimal values stored in the control system according to the measured atmospheric conditions. Finally, the control is adjusted to reach the optimal power value【10】.

Among these methods, we can mention:

- The curve fitting method

- The look-up table method

- The open-circuit voltage method

- The short-circuit current method

III.4.2 Direct Methods (Online Methods)

Direct methods are iterative algorithms that search for the optimal value of V_{pv} to ensure that the PV generator delivers its maximum power. The advantage of these algorithms is that they do not require prior knowledge of the characteristics of the PV panels. In the literature, many MPPT algorithms exist, such as the Perturb and Observe (P&O) method, the Incremental Conductance (Inc-Cond) method, Hill Climbing, among others.

III.4.2.1 P&O Method

The Perturb and Observe (P&O) method is one of the most widely used MPPT techniques. It is an iterative method that seeks to find the Maximum Power Point (MPP). The basic idea of this technique is to measure the characteristics of the PV panel and then introduce a small

perturbation to the voltage (or current) to analyze the resulting change in power【3】. For example, if the injected perturbation is positive and the delivered power increases, the voltage is further increased in the same direction. If the power does not increase, the voltage is decreased (opposite direction).Figure III-3 and Figure III-4illustrate this principle in detail.

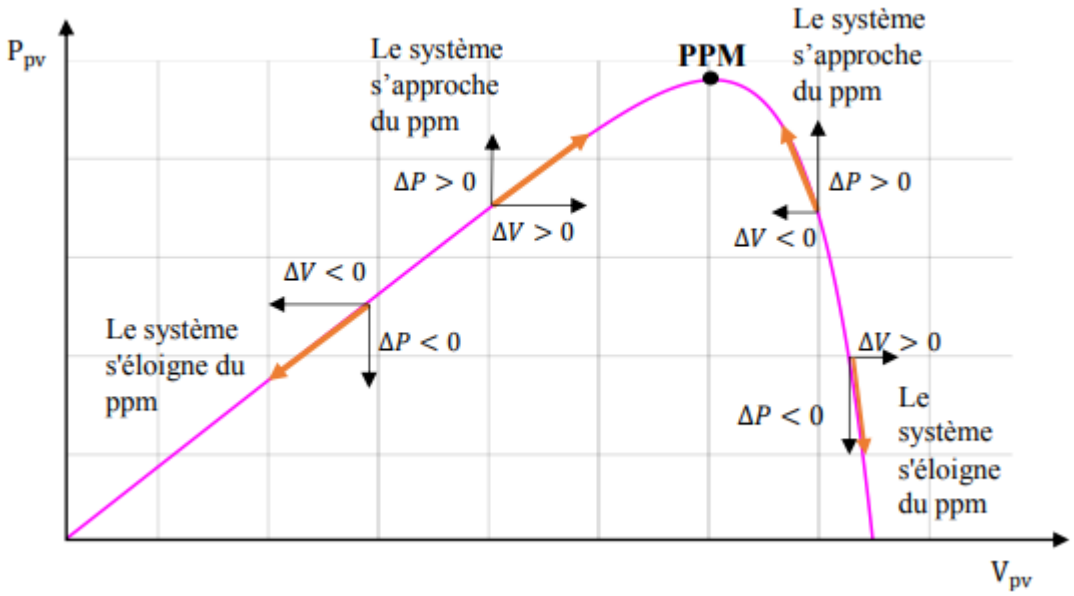

Figure III-12 Principle of the P&O Method.

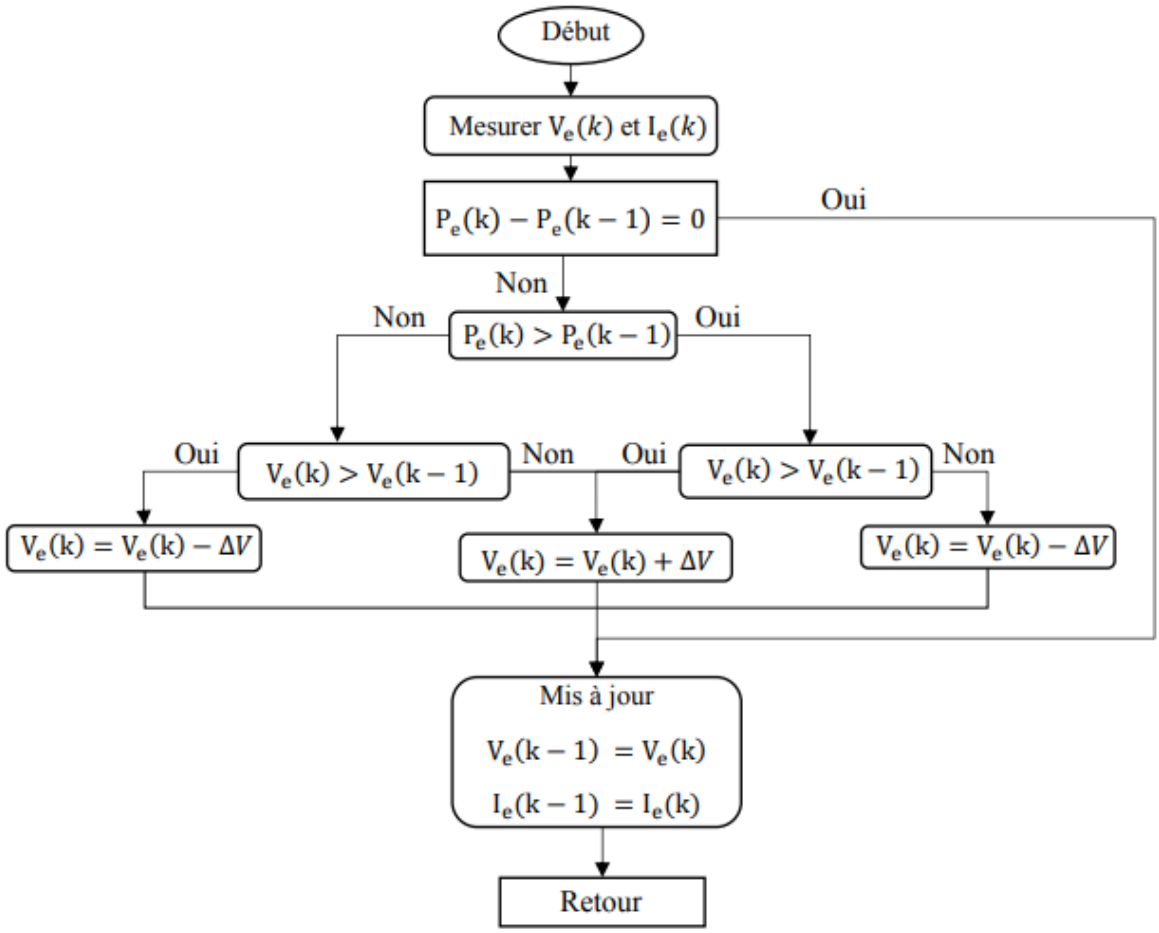

Figure III-13 Flowchart of the P&O Method.

- **Disadvantages of the P&O Method**

The P&O algorithm has the following two disadvantages:

- Sudden Changes in Irradiation: During sudden changes in irradiation, the algorithm may temporarily move away from the MPP and can potentially lose control permanently.
- Oscillations Around the MPP: Another drawback of the P&O algorithm is the oscillations around the MPP. Reducing the increment step (Δ V) can be considered a solution to decrease these oscillations. However, this solution slows down the tracking of the MPP. Therefore, a compromise must be made between accuracy and speed.

III.4.2.2 IncCond Method

The Incremental Conductance (IncCond) method was developed to address the disadvantages of the P&O method, particularly in dealing with sudden changes in climatic conditions. The principle of the IncCond method is based on the cancellation of the derivative of power with respect to voltage. The principle is as follows:

$$\frac{dP}{dV} = \frac{dP}{dV} I + \frac{dI}{dV} V = I + \frac{dI}{dV} V \tag{III.32}$$

$$P_{pv} = P_{max} \Rightarrow I + \frac{dI}{dV} V = 0 \Rightarrow \frac{dI}{dV} = -\frac{I}{V} \tag{III.33}$$

If:

$$\frac{\Delta I}{\Delta V} > -\frac{I}{V} \tag{III.34}$$

then the MPP is to the right of the current operating point.

If:

$$\frac{\Delta I}{\Delta V} < -\frac{I}{V} \tag{III.35}$$

then the MPP is to the left of the current operating point.

If:

$$\frac{\Delta I}{\Delta V} = -\frac{I}{V} \tag{III.36}$$

then the operating point is at the MPP.

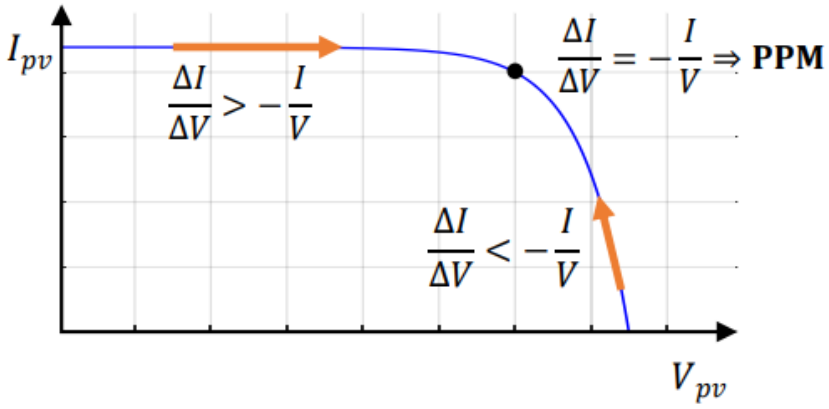

Figure III-14Principle of the IncCond Method..

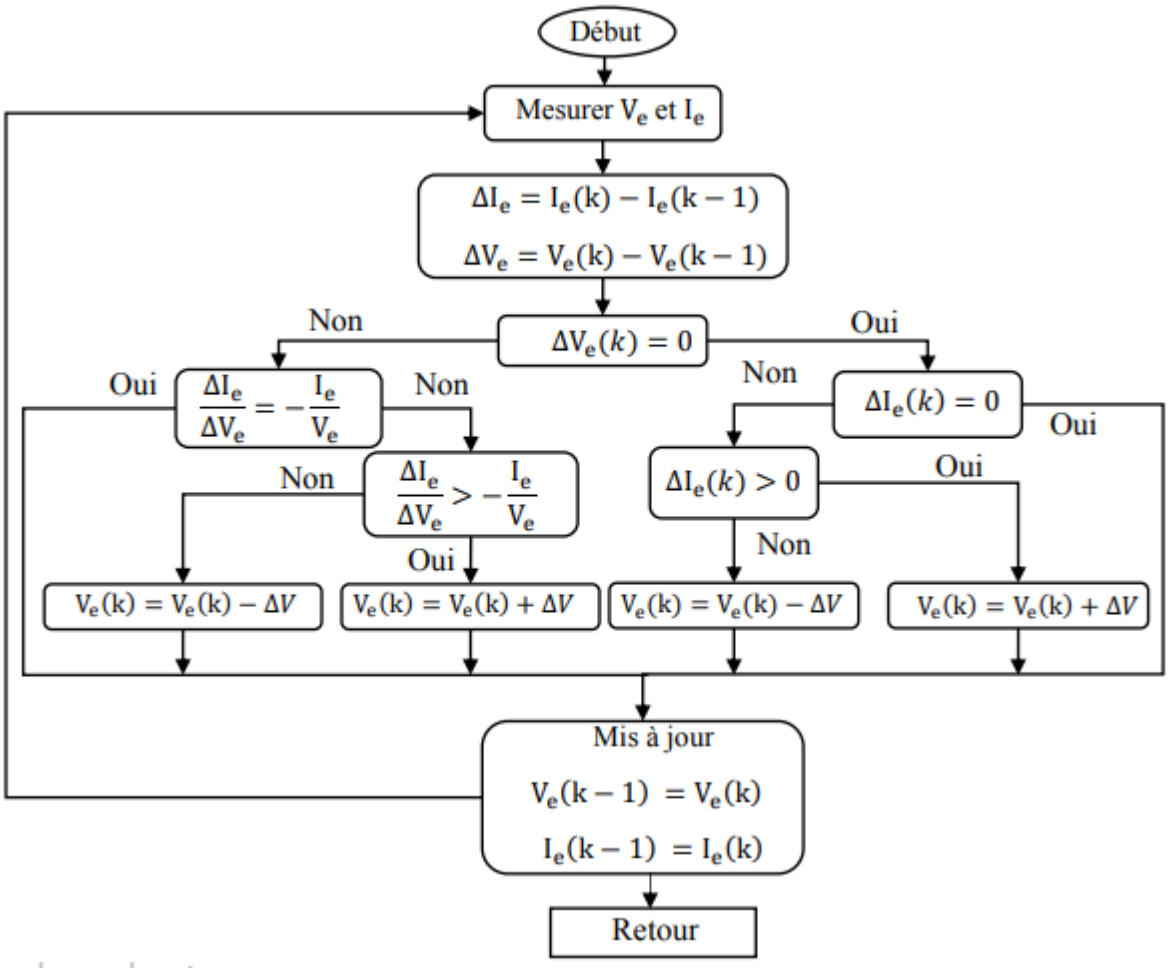

Figure III-15 Flowchart of the IncCond Method.

- Disadvantages of the IncCond Method

This algorithm faces implementation challenges due to the complexity of the control circuit, and the real-time calculation of the derivative requires a fast processor.

III.4.2.3 Simulation of P&O and IncCond Algorithms

The objective of this section is to simulate the MPPT algorithms (P&O and IncCond) for a PV generator connected to a resistive load through a DC/DC converter. In the first simulation, a Buck converter is used, and in the second simulation, a Boost converter is utilized.

- First Simulation

In this simulation, we consider the PV generator described in the following parameters Table II.1 and the Boost converter shown in Figure III.9. The temperature is fixed at 25°C, and the illumination varies as depicted in Figure II.17. The converter parameters are as follows: C_1 = 200e^{-6} mu F;C_2 = 1000 mu F , L = 3.5e^{-3}mH , and R = 300 Ω . The initial conditions V_{pv}, I_L, V_s \)) are assumed to be zero. The switch is closed in the initial state α0 = 1. The reference power is determined by a simple algorithm that increments the voltage V_e to analyze the resulting power variation. The simulation results are shown in Figures

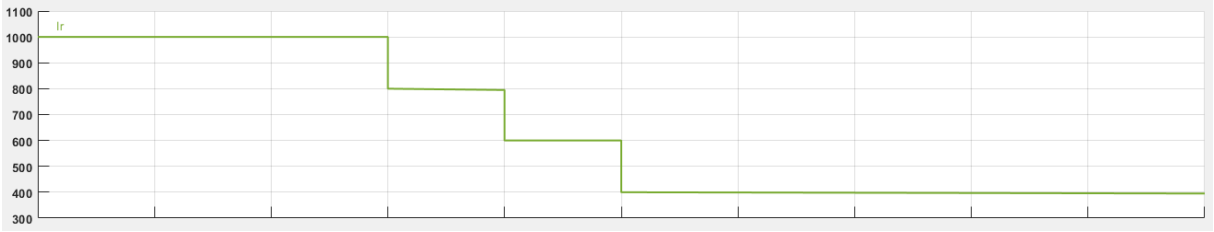

Figure III-16 Variation in Irradiation

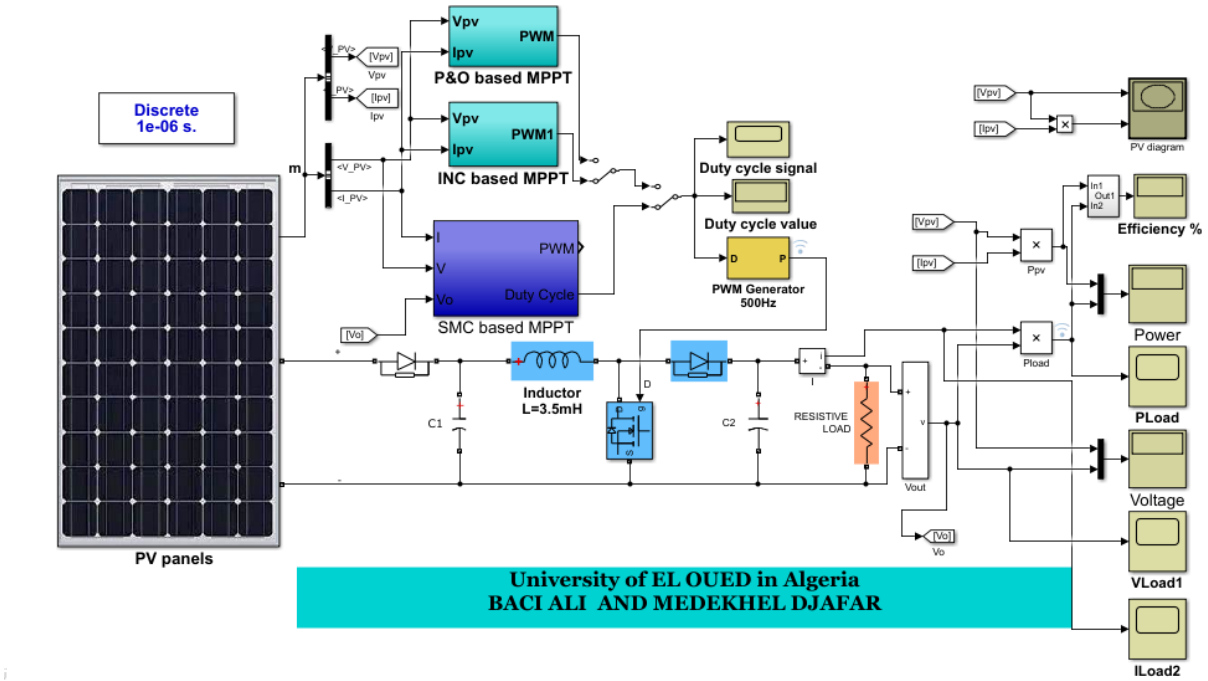

Figure III-17 Simulation Results for PV Generator and Boost Converter

Perturb and Observe (P&O) Simulation of the First PV System

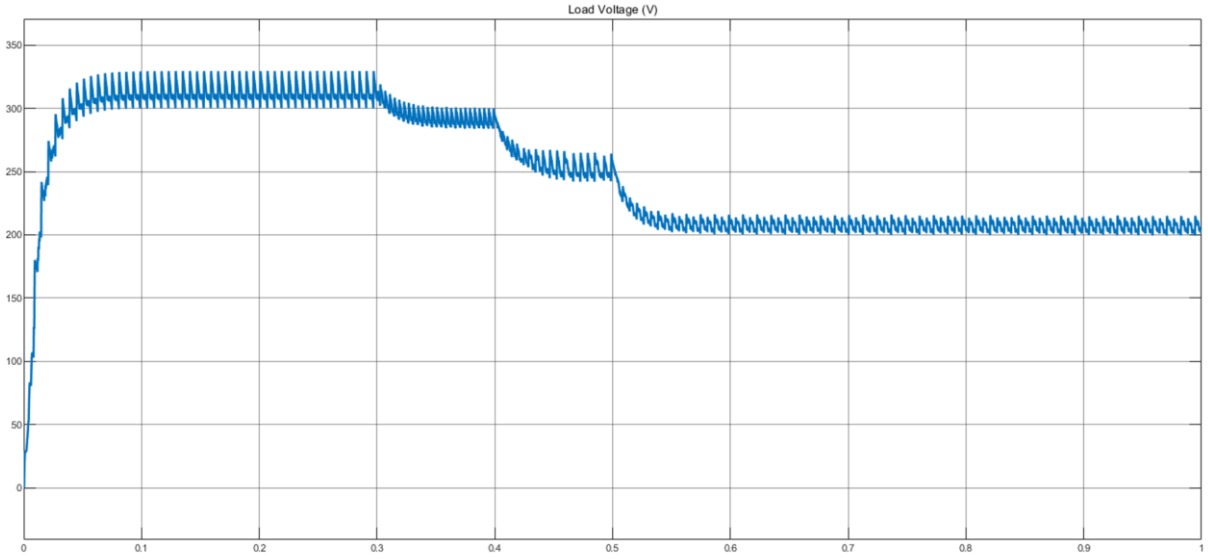

Figure III-18 Voltage across the load.

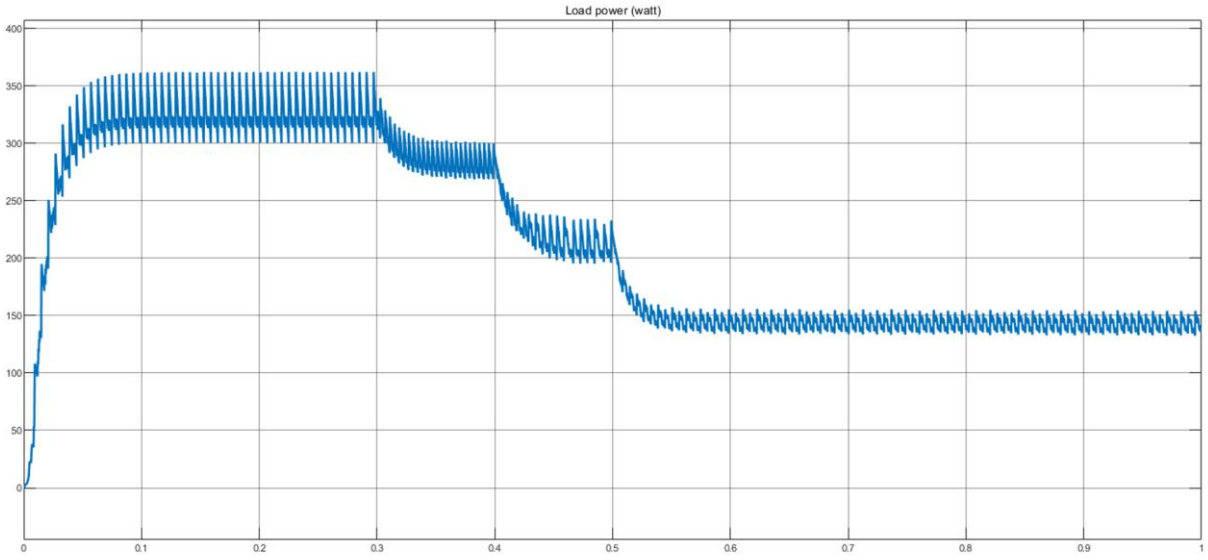

Figure III-19 Power received by the load.

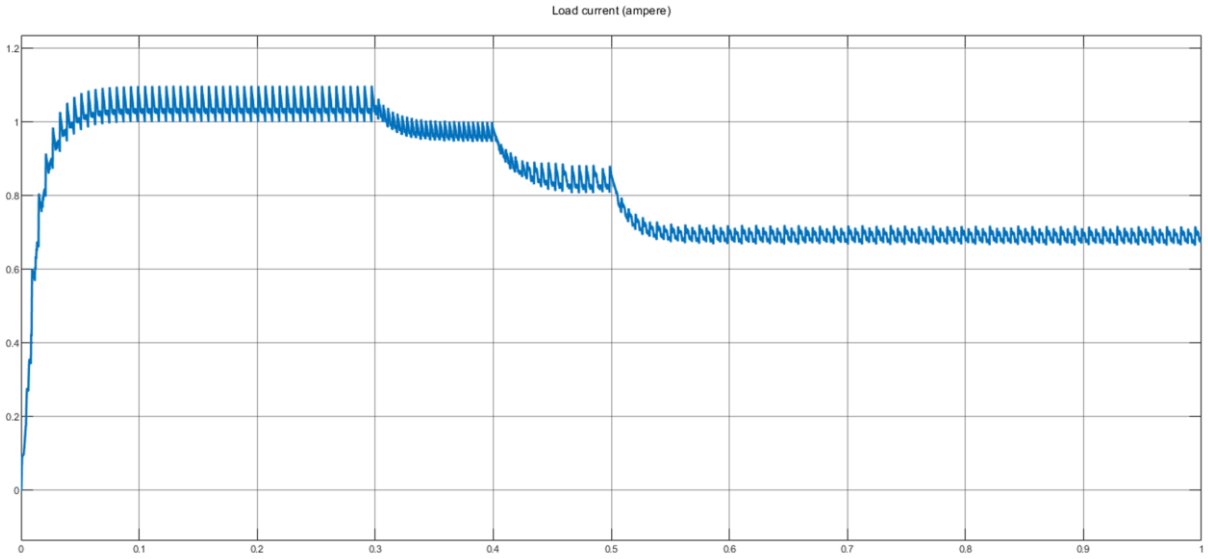

Figure III-20 current flowing into the load

Incremental Conductance (IncCond) Simulation of the second PV System

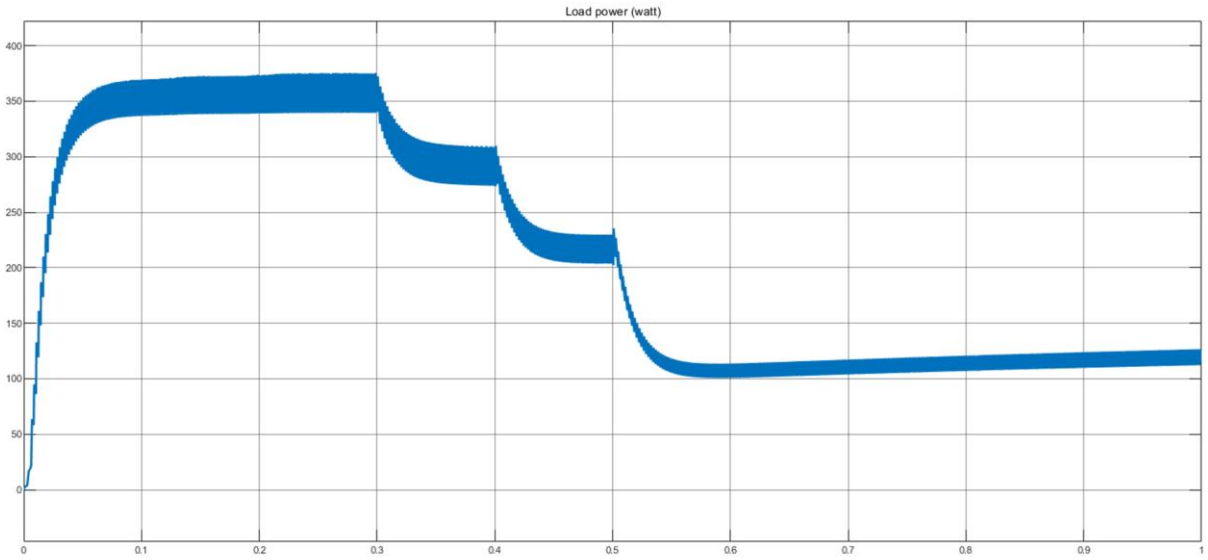

Figure III-21 Power received by the load.

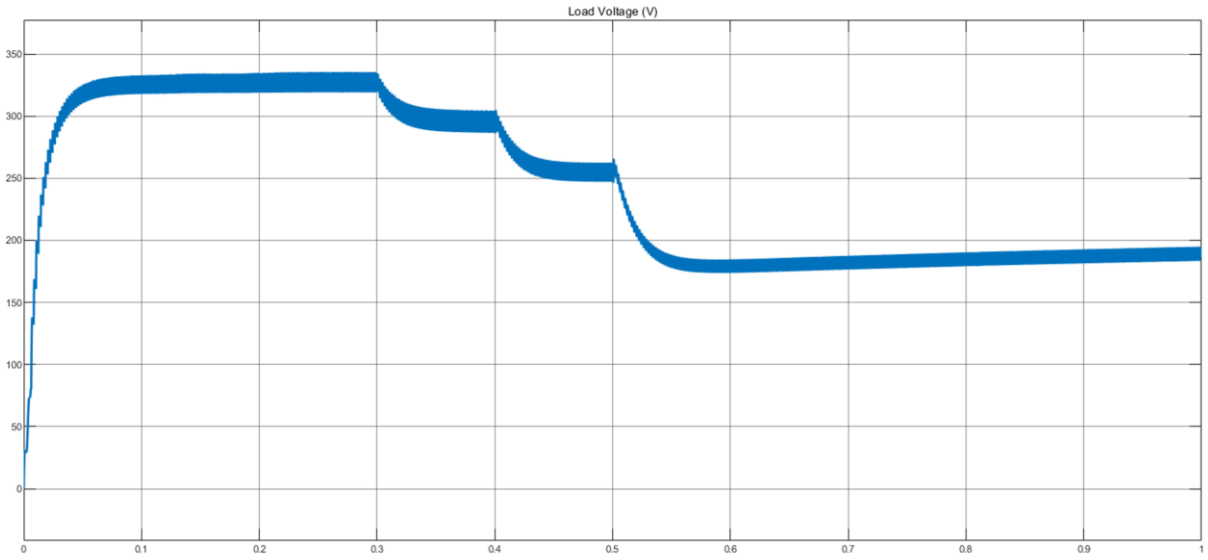

Figure III-22Voltage across the load.

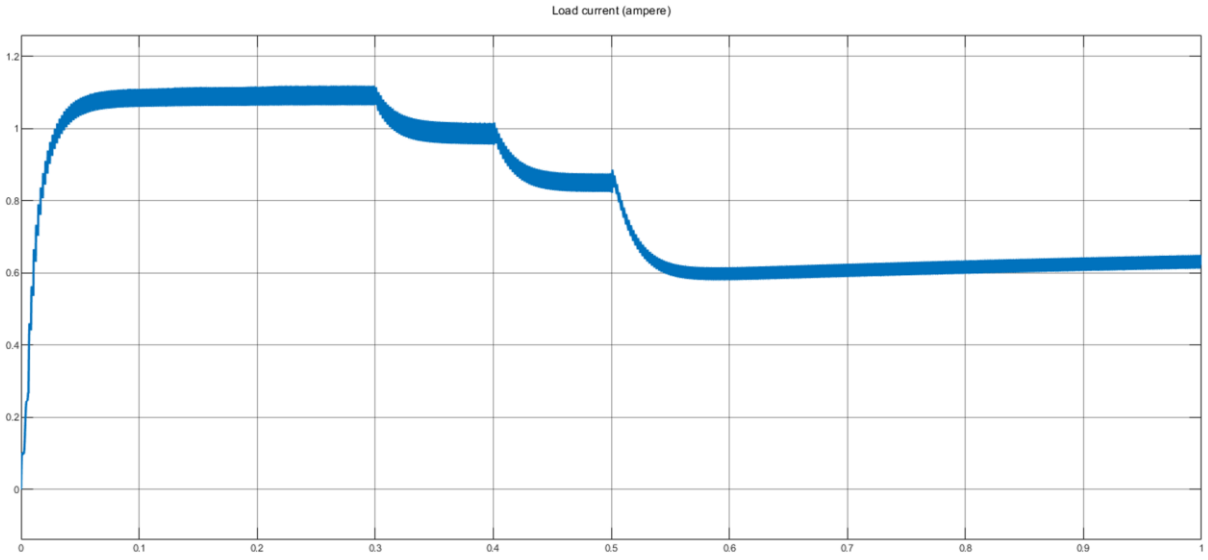

Figure III-23 urrent flowing into the load.

Discussion of Results

Based on the results obtained from the simulation, it is observed that the maximum power point is reached very quickly (approximately 0.1 seconds for the Boost). The control signal value (duty cycle) varies between 0 and 1 (switch open/switch closed) with small oscillations.

III.5. Conclusion

In this chapter, we addressed the connection between the photovoltaic generator and the load, either through direct connection or via an adaptation stage. Adjusting the voltage of the PV generator requires the use of an adaptation stage, which is a DC/DC converter controlled by MPPT algorithms. In this chapter, we simulated two algorithms (P&O and IncCond). The simulation results demonstrate the speed of these algorithms. However, these conventional algorithms have drawbacks such as sensitivity to abrupt changes in illumination (robustness issue) and oscillations around the maximum power point.

Chapter IV
Sliding Mode controller based MPPT of PV water pumping system

IV.1. Introduction

Sliding mode control (SMC) is one of the widely used nonlinear control techniques, celebrated for its simplicity of implementation and robustness against uncertainties and external disturbances.

In this chapter, we will present the foundational and theoretical aspects of sliding mode control. Following this, we will apply the approach to PV systems to ensure optimal operation. Finally, we will simulate this approach using the Matlab environment.

IV.2. Principle of Sliding Mode Control

The principle of sliding mode control (SMC) involves driving the system state to reach a desired sliding surface from any point in the phase plane. Once the surface is reached, the system slides along this surface towards the equilibrium point, as illustrated in Figure IV-1

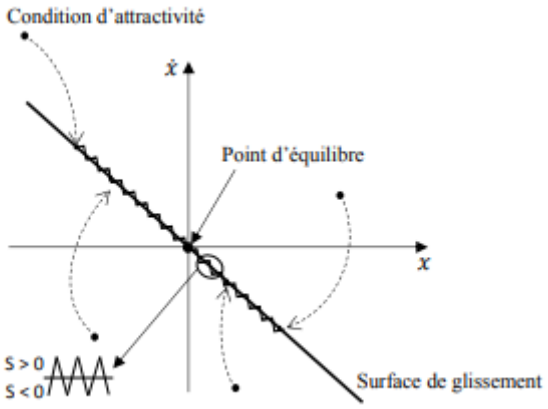

Figure IV-1Phase Diagrams in Sliding Mode

In Sliding Mode Control Theory, the System Dynamics Have Two Sequential Modes:

- **Reaching Mode (Mode de Convergence):**The reaching mode corresponds to the period during which the state trajectories of the system move towards the sliding surface. During this phase, the system is sensitive to parameter variations and external disturbances. The control law applied in this mode is designed to drive the system state from its initial condition to the sliding surface in finite time.

- **Sliding Mode (Mode de Glissement):**In the sliding mode, the state trajectories remain on the sliding surface. The system's behavior in this mode is entirely determined by the choice of the sliding surface, which dictates the reduced-order dynamics. This phase is characterized by robustness to parameter variations and external disturbances, as the control input continuously adjusts to maintain the system state on the sliding surface.

IV.3. Synthesis of the Sliding Mode Control Law

Consider the following nonlinear system:

$$\dot{x}(t) = f(x) + g(x)u \qquad \text{(IV. 1)}$$

Where $x(t)$ represents the system state, u is the control input, $f(x)$ and $g(x) \neq 0$ are known nonlinear functions. The control objective is to compel the system output $y(t)$ to follow a desired trajectory $yd(t)$. The first step to achieve this is to choose a sliding surface that represents the desired dynamics. The simplest surface is a hyperplane passing through the origin of the state space. A general formula for determining the sliding surface is provided as follows [25]:

$$s(x) = \left(\frac{d}{dt} + \lambda\right)^{n-1} e(x) \qquad \text{(IV.2)}$$

Where:

• $e(x) = y - yd$: represents the tracking error.

• λ: is a positive constant representing the sliding slope.

• n: relative degree, equal to the number of times the output needs to be differentiated to reveal the control.

For the system to reach this surface, a necessary condition, called the attractiveness condition, must be satisfied, and it is given as follows:

$$s\dot{s} < 0 \tag{IV.3}$$

Cependant, l'inégalité précédente n'est pas suffisante pour assurer une convergence en temps

Towards reaching the surface. Therefore, this condition is generally replaced by the condition, known as the η-attractiveness condition [26]:

$$s\dot{s} < -\eta|s|, \eta > 0 \tag{IV.4}$$

The condition (III.4) ensures finite-time convergence ($ts \leq |s(0)|/\eta$) to the surface $s(t, x) = 0$.

The next step is the design of the control law. According to the equivalent method, the control law consists of two components (one discontinuous and the other continuous) as follows:

$$u = u_{sw} + u_{eq} \tag{IV.5}$$

The discontinuous component u_{sw} of the control brings the trajectories back to the sliding surface and ensures robustness against uncertainties and external disturbances. Its mathematical formula is given as follows:

$$u_{sw} = -k\left(\frac{\partial s}{\partial x}g(x)\right)^{-1}\text{sign(s)} \tag{IV.6}$$

Where:

• K: a positive constant,

•sgn: the discontinuous (sign) function shown in the following figure:

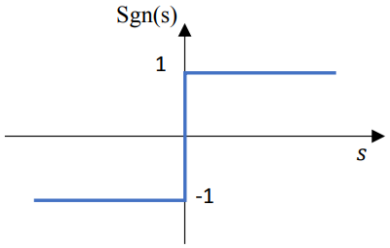

Figure IV-2Sign Function

Once the system reaches the sliding surface, the role of the equivalent control ueq comes into play, which keeps the system sliding along this surface. This equivalent control is obtained through the following invariance conditions [27]:

$$s = \dot{s} = \left(\frac{\partial s}{\partial x}\right)\left(f(x) + g(x)u_{eq}\right) = 0 \qquad \text{(IV.7)}$$

D'après l'équation III.7, on peut définir la commande équivalente comme suit :

$$u_{eq} = -\left(\left(\frac{\partial s}{\partial x}\right)^T g(x)\right)^{-1} - \left(\left(\frac{\partial s}{\partial x}\right)^T f(x) + \frac{\partial s}{\partial t}\right) \qquad \text{(IV.8)}$$

The equivalent control can be interpreted as the average value of the control during the rapid switching between $u + et$ and u - as shown in Figure IV-2

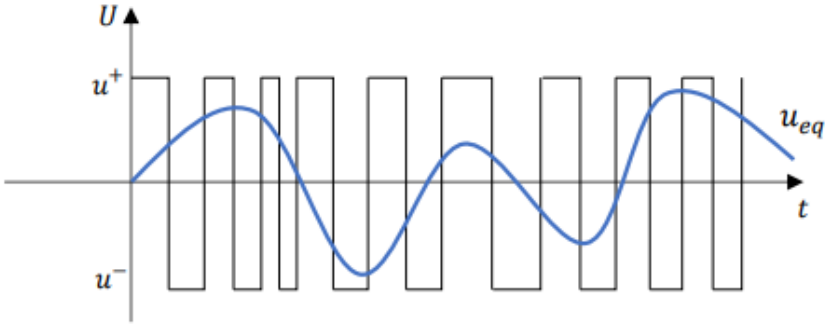

Figure IV-3 Equivqlent command

IV.4. Chattering Phenomenon

The chattering phenomenon (or bouncing or in English chattering) is caused by the discontinuous term usw of the sliding mode control, which excites strong oscillations around the surface and the control signal (see Figure IV-3). Indeed, the discontinuous term is effectively applied when the system leaves the surface due to the delay in output measurement. This delay

can be amplified if the system naturally exhibits delays or neglected dynamics. Another cause of chattering, particularly in control, is measurement noise.

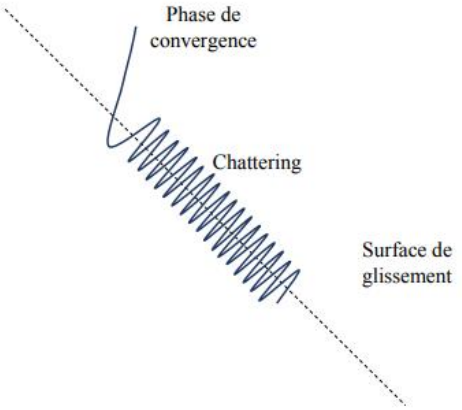

Figure IV-4 Phénomène de broutement

This phenomenon is undesirable because, even if filtered at the output of the process, it can excite unmodulated high-frequency modes, which degrade system performance and may even lead to instability [28]. Chattering in control also causes significant wear on actuators or certain parts of the system, and significant heat losses in electrical circuits.

Several procedures have been designed to reduce or eliminate this chattering. Among these solutions are:

❖Slotine's proposal (or the boundary layer) [25], which involves replacing the sign function $signe(.)$ with continuous approximations such as saturation functions $\boldsymbol{sat}(\boldsymbol{s}/\boldsymbol{\varepsilon})$, hyperbolic tangent $\boldsymbol{tanh}(\boldsymbol{s}/\boldsymbol{\varepsilon})$, etc.

$$sat(^{s}/_{\Phi}) = \begin{cases} ^{s}/_{\Phi} & si\ |s| \leq \Phi \\ sgn(s) & autre \end{cases}$$

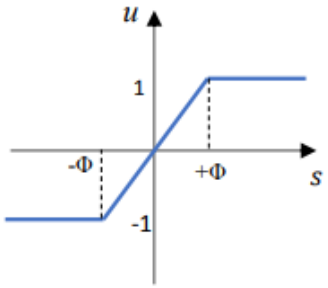

$$tanh(^{s}/_{\varepsilon}) = \begin{cases} \tanh(s) & si\ |s| \le \delta \\ sgn(s) & sinon \end{cases}$$

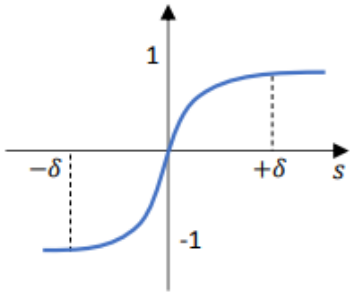

❖Another solution involves replacing the first-order sliding mode "$s = 0$" with a higher-order sliding mode "$s = s^{(1)} = \cdots = s^{(n)} = 0$" where n is the order of the sliding mode.

❖ There is also a solution based on using an observer that generates the ideal sliding mode in an auxiliary loop. However, this solution has encountered the problem of asymptotic convergence of the estimated state to the real system state and the observer does not take into account unmodeled disturbances [26].

❖ Another method to reduce chattering involves replacing the discontinuous component (usw) with a fuzzy PI controller.

$$usw = k_p s + k_i \int sdt \qquad (IV.9)$$

Where:$s = \theta_p{}^T \delta(z)$, $\theta p = [kp, ki]^T$

is the vector of adjustable parameters, $\delta(z)$ is the vector of fuzzy base functions with z=$[z_1,z_2]^T$,

such that $z_1 = s$ and $\dot{z}_2$ =S

IV.5. Sliding Mode Control of PV Systems

In this section, we focus on the application of sliding mode control for two PV systems. The first PV system consists of a PV generator connected to a Buck converter. However, in the second PV system, the PV generator is connected to a Boost converter.

The objective of the control for both PV systems is to ensure maximum power transfer provided by the PV generator to the load. In other words, control the duty cycle of the converter such that the power supplied by the PV generator follows a desired maximum power generated by a reference system.

IV.5.1 Reference System

The objective of this section is to find the mathematical expression of the output of the reference system, i.e., to deduce the equation of the desired maximum power.

To achieve this objective, we set the derivative of the power with respect to the output current Ipv to zero, as shown in the following equation:

$$\frac{dP}{dI_{pv}} = \frac{d}{dI_{pv}}(V_{pv}I_{pv}) = V_{pv} + \frac{dV_{pv}}{dI_{pv}}I_{pv} = 0 \quad \text{(IV.10)}$$

To simplify the calculation of the derivative, we consider the simplified model of the PV generator given by (II.1), then invert it to obtain the output voltage Vpv as follows:

$$V_{pv} = nVt.log\left(\frac{I_{ph} - I_{pv} + I_{sat}}{I_{sat}}\right) \quad \text{(IV.11)}$$

We differentiate the voltage Vpv (IV.11) with respect to the current Ipv, obtaining:

$$\frac{\partial V_{pv}}{\partial I_{pv}} = -nVt\frac{1}{I_{ph} - I_{pv} + I_{sat}} \quad \text{(IV.12)}$$

Using (IV.12), equation (IV.10) becomes as follows:

$$I_{pv} - (I_{ph} - I_{pv} + I_{sat})log\left(\frac{I_{ph} - I_{pv} + I_{sat}}{I_{sat}}\right) = 0 \quad \text{(IV.13)}$$

Solving equation (IV.13), we get:

$$I_{pv\_max} = 0.909I_{ph} \quad \text{(IV.14)}$$

$$V_{pv\_max} = nVt.log\left(\frac{I_{ph} - I_{pv\_max} + I_{sat}}{I_{sat}}\right) \quad \text{(IV.15)}$$

where $\mathbf{V_{pv_max}}$and$\mathbf{I_{pv_max}}$are the values of voltage and current, respectively, when the PV array reaches its maximum power. Consequently, the equation for the maximum power is given as follows:

$$P_{pv\_max} = V_{pv\_max}.I_{pv\_max} \quad \text{(IV.16)}$$

IV.5.2 Sliding Mode Control for the First PV System

We consider the PV generator given by (III.1) and the Buck converter given by (III.9andIII.10and III 11). The objective of the sliding mode control is to find the duty cycle (\(

u = \alpha \)) of the converter that enables the generated power of the PV system to converge to the sliding surface (\(S = 0 \)) provided below and then maintain it along this surface.

IV.5.3 Sliding Surface

For this first PV system, our sliding surface is chosen as follows:

$$S(x) = \frac{dP_{pv}}{dV_{pv}} = I_{pv} + \frac{dI_{pv}}{dV_{pv}} V_{pv} \quad \text{(IV.17)}$$

Where $x = [x_1; x_2; x_3] = [V_{pv}; I_L; V_s]$.

We use the equation of the PV system (III1), the surface (III.17) becomes as follows:

$$S(x) = N_p I_{cc} - \left(N_p I_{cc} + \frac{N_p I_{cc}}{nV_T} V_{pv}\right) exp\left(\frac{V_{pv} - N_s V_{co}}{nV_T}\right) \quad \text{(IV.18)}$$

At the maximum power point, we have:

$$S(x) = 0 \quad \text{(IV.19)}$$

The time derivative of the surface (III.19) is given as follows:

$$\dot{S}(x) = \frac{dS}{dt} = \frac{\partial S}{\partial x}\frac{\partial x}{\partial t} = \frac{dS}{dx}\dot{x} = \frac{\partial S}{\partial V_{pv}}\dot{V}_{pv} + \frac{\partial S}{\partial I_L}\dot{I}_L + \frac{\partial S}{\partial V_s}\dot{V}_s \quad \text{(IV.20)}$$

According to the Buck converter model (II.5), we have: $\frac{\partial S}{\partial I_L} = \frac{\partial S}{\partial V_s} = 0$ nd $\frac{\partial S}{\partial V_{pv}} \neq 0$

Therefore, the dynamics (IV.20) become as follows:

$$\begin{gathered} \dot{S}(x) = \frac{\partial S}{\partial V_{pv}}\dot{V}_{pv} \\ \dot{V}_{pv} = \frac{1}{C1} I_{pv} - \frac{\alpha}{C1} I_L \\ \frac{\partial S}{\partial V_{pv}} = \left(\frac{-2N_p I_{sat}}{nVt} exp\left(\frac{V_{pv} - N_s V_{co}}{nVt}\right) - \frac{N_p I_{sat}}{(nVt)^2} exp\left(\frac{V_{pv} - N_s V_{co}}{nVt}\right)\right) \end{gathered} \quad \text{(IV.21)}$$

IV.5.3.1 Control law synthesis

According to the principle of the sliding mode approach, we define the control law as follows:

$$u = u_{eq} - u_{sw} \quad \text{(IV.22)}$$

With

$$u_{sw} = \frac{\gamma}{I_L}.sign(S) \quad \text{(IV.23)}$$

Where $\gamma$is a positive constant.

The term ueq represents the equivalent command calculated by setting:

$$S = \dot{S} = \frac{\partial S}{\partial V_{pv}}\dot{V}_{pv} = 0 \quad \text{(IV.24)}$$

Since the term $\frac{\partial S}{\partial V_{pv}}$ictly negative, we deduce that:

$$\dot{V}_{pv} = \frac{1}{C1}I_{pv} - \frac{u}{C1}I_L = 0 \quad \text{(IV.25)}$$

And consequently, we obtain:

$$u_{eq} = \frac{I_{pv}}{I_L} \quad \text{(IV.26)}$$

IV.5.3.2 Verification of Existence Condition

To verify the existence condition (analyze stability), we consider the following Lyapunov function:

$$V(x) = \frac{1}{2}S^2 \quad \text{(IV.27)}$$

And consequently, we obtain:

$$\dot{V} = S\dot{S} = S\left(\frac{\partial S}{\partial V_{pv}}\dot{V}_{pv}\right) = S\frac{\partial S}{\partial V_{pv}}(\frac{1}{C1}I_{pv} - \frac{u_{eq}-u_{sw}}{C1}I_L) \quad \text{(IV.28)}$$

En substituant les termes u_{sw}et u_{eq}par leurs formules (IV.23) et (IV.26), respectivement, l'équation (IV.28) devient :

$$\dot{V} = |S|\frac{\partial S}{\partial V_{pv}}\frac{\gamma}{C1} < 0 \quad \text{(IV.29)}$$

From equation (IV.29), we can conclude that the η-attractiveness condition is satisfied, and the photovoltaic generator (GPV) converges to its maximum power in finite time.

III.5.3. Sliding Mode Control for the Second PV System

Indeed, the sliding mode control approach presented for the control of the first PV system is not useful for the second PV system because the control signal does not appear in the expression of the sliding surface dynamics. To solve the problem of applying the sliding mode control approach to this second PV system, the control objective becomes to force the output voltage **Vpv** of the PV generator (GPV) to follow its optimal voltage $\mathbf{V_{pv\_max}}$ given by (IV.15).

To implement this control, we start by defining the following errors:

$$e_1 = V_{pv} - V_{pv\_max} \tag{IV.30}$$

$$e_2 = I_l - I_{l_{ref}} \tag{IV.31}$$

Where $I_{l_{ref}} = I_{pv} - c1 * \dot{V}_{pv\_max}$.

We consider the PV model presented in (II.2) and the Boost converter given in (III.9andIII.10andIII.11), then we differentiate errors (IV.30) and (IV.31) with respect to time, obtaining:

$$\dot{e}_1 = \dot{V}_{pv} - \dot{V}_{pv\_max} = \frac{1}{c1}(I_{pv} - I_l) - \dot{V}_{pv\_max} = \frac{-e_2}{c1} \tag{IV.32}$$

$$\dot{e}_2 = I_l - \dot{I}_{l_{ref}} = \frac{1}{\mathrm{L}}(Ve - (1-\alpha)Vs) - \dot{I}_{l_{ref}} = f + \alpha g \tag{IV.33}$$

Where $f = \frac{1}{\mathrm{L}}(V_{pv} - V_s) - \dot{I}_{l_{ref}}$, $g = \frac{\alpha}{\mathrm{L}} V_s$ et $\dot{I}_{l_{ref}} = \frac{\partial I_{pv}}{\partial V_{pv}} \dot{V}_{pv} - c1 * \dot{V}_{pv\_max}$.

We denote $z1 = -c1 * e1$ and $z2 = e2$, then we obtain the following normal form:

$$\dot{z}_1 = z_2$$
$$\dot{z}_2 = f + \alpha g \tag{IV.34}$$

III.5.3.1. Sliding surface:

From the system (IV.35), we consider the following sliding surface:

$$S = \dot{z}_1 + \lambda z_1 \tag{IV.35}$$

where λ is a positive constant.

The time derivative of this surface is given as follows:

$$\dot{S} = \ddot{z}_1 + \lambda \dot{z}_1 = f + \alpha g + \lambda z_2 \tag{IV.36}$$

III.5.3.2. Synthesis of the control law

In the same way as for the first PV system, the control law is defined as follows:

$$u = u_{eq} - u_{sw} \tag{IV.37}$$

With

$$u_{sw} = \frac{\gamma}{g}.sign(S) \tag{IV.38}$$

Where γ is a negative constant.

We use the invariance conditions **(S = $\dot{S}$ = 0),** the equivalent command u_{eq} is determined as follows:

$$u_{eq} = \frac{-f-\lambda z_2}{g} \tag{IV.39}$$

III.5.3.3. Verification of the existence condition

To verify the existence condition, we consider the following Lyapunov function:

$$V(x) = \frac{1}{2}S^2 \tag{IV.40}$$

The time derivative of this function is given by:

$$\dot{V} = S\dot{S} = S(f + (u_{eq} - u_{sw})g + \lambda z_2 \tag{IV.41}$$

We use the expressions (IV.38) and (IV.39), equation (IV.41) becomes as follows:

$$\dot{V} = -\gamma|S| < 0 \quad \text{(IV.42)}$$

According to equation (IV.42), we can conclude that the η-attractiveness condition is satisfied and the output voltage V_{pv} asymptotically converges to its optimal voltage V_{pv_max}. Consequently, the PV system generates its maximum power.

3.4 DC Motor and Pump

Using DC motors in PV pumping systems instead of AC motors has been the subject of many studies. These studies concluded that DC motors can be directly coupled to the PV array, significantly reducing the overall system cost and complexity. In this work, a permanent magnet DC motor (PMDCM) is proposed. PMDCMs are reliable, efficient, and require low maintenance【30】. Additionally, when coupled with a centrifugal pump, they have matching characteristics suitable for the PV array and possess a low starting torque compared to other PV electro-mechanical systems.

3.4.1 PMDC Motor Modelling

The equivalent circuit of the permanent magnet DC motor (PMDCM) is depicted in Figure IV-4 【30】. In this circuit:

- R_a represents the armature winding resistance (Ω),
- L_a is the armature self-inductance (H),
- $I_a$denotes the motor armature current (A), and
- $V_a$is the applied voltage (V).

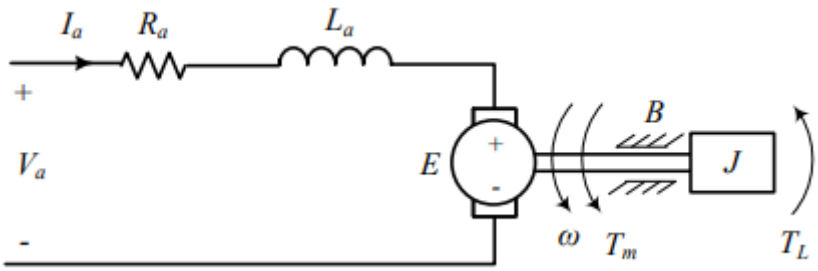

Figure IV-5 Circuit Model for DC Permanent Magnet Motor with Pump Load

From the equivalent circuit shown in Fig. IV-5, the armature DC voltage can be calculated by using Equation (IV.43).

$$V_a = R_a I_a + L_a \frac{dI_a}{dt} + e \tag{IV.43}$$

The induced voltage **e** is generated when the motor is running and is referred to as the back electromotive force (emf) or counter electromotive force. This induced voltage e is directly proportional to the angular speed of the rotor Ωm, the proportionality constant K_e, and the field flux Ω, as expressed in Equation (IV.44).

$$e = K_e \Phi \omega_m \tag{IV.44}$$

In the case of separately exited motors with constant field voltage or permanent magnet motors the field flux remains constant. Accordingly, Equation (IV.44) becomes;

$$e = K_e \omega_m \tag{IV.45}$$

Hence Equation (IV.43) becomes;

$$V_a = R_a I_a + L_a \frac{dI_a}{dt} + K_e \omega_m \tag{IV.46}$$

The torque balance equation is given by

$$T_e = J \frac{d\omega_m}{dt} + B_m \omega_m + T_L \tag{IV.47}$$

Where J is the moment of inertia, B_m is the viscous torque constant for rotational losses, T_e and T_L are the electromagnetic torque and the load torque respectively. The electromagnetic torque

T_e is equal to the product of the torque constant K_t and the current through the armature winding as given by:

$$T_e = K_t I_a \tag{IV.48}$$

Therefore Equation (IV.47) can be rewritten as:

$$K_t I_a = J \frac{d\omega_m}{dt} + B_m \omega_m + T_L \tag{IV.49}$$

For a constant flux machine the torque constant is equal to the back emf constant (Ke) [31].

Also the torque developed by the armature can be written as in Equation (IV.50).

$$T_e = \frac{P_e}{\omega_m} = \frac{e\, I_a}{\omega_m} = \frac{K_e \omega_m\, I_a}{\omega_m} = K_t I_a \tag{IV.50}$$

In a steady-state condition, Equations (IV.43) and (IV.47) become:

$$V_a = R_a I_a + E \tag{IV.51}$$

$$K_t I_a = B_m \omega_m + T_L \tag{IV.52}$$

3.4.2 Direct Coupling of the DC Motor

Coupling the DC motor directly to the PV array in a water pumping system without any interfacing circuitry results in significant efficiency losses. This is due to the deviation of the operating point from the optimal point, as shown in FigIV-6.

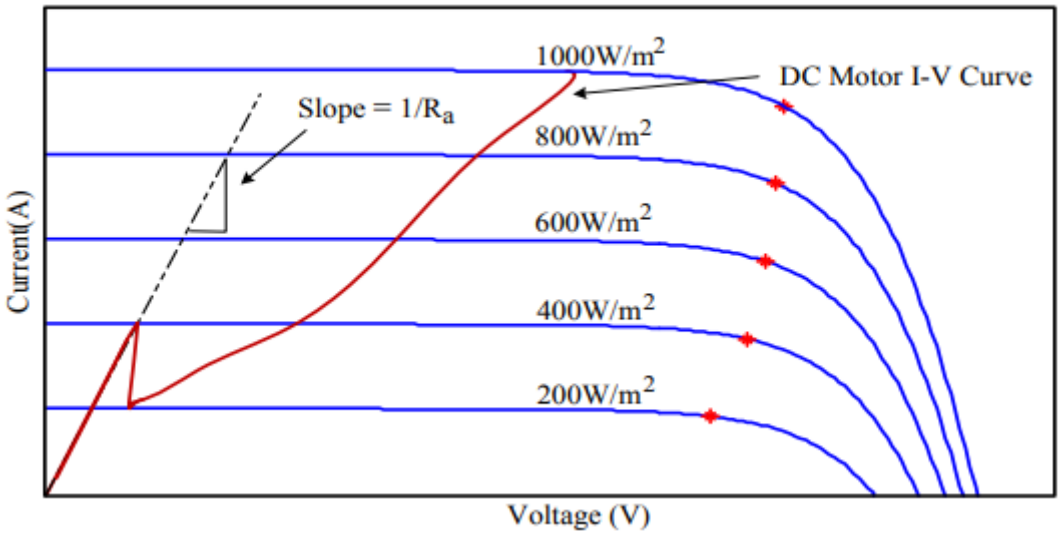

Figure IV-6 PV I-V Curves at Different Irradiation Levels and a DC Motor I-V Curve

It's evident that the motor won't start running until it receives an irradiation of 400W/m2. However, once it starts, it can maintain minimum operation with just 200W/m2 of irradiation. This limitation means that the system can't make full use of morning sunlight because there isn't enough starting torque. As a result, the motor may remain locked for extended periods, causing electrical energy input to be converted into heat instead of mechanical output, thereby shortening the motor's lifespan. To address this issue, a device called a linear current booster (LCB) is designed. Additionally, in direct coupling, changes in irradiance or PV array operating temperature often result in the DC motor operating far from its maximum operating point. This problem can be mitigated by using a DC-DC converter as an interface, allowing the operating point of the PV array to be adjusted to the maximum power point. The converter achieves this by altering the input resistance through changes in the duty ratio.[32].

3.4.3 Interfacing the PV array to the DC water pumping load

This section presents how to maximize the power delivered from the PV array to the load at all insolation levels. A buck converter without the output filter, which is essentially a step-down converter, also known as a chopper, inserted between the PV array and the load as shown in Fig. IV-7.

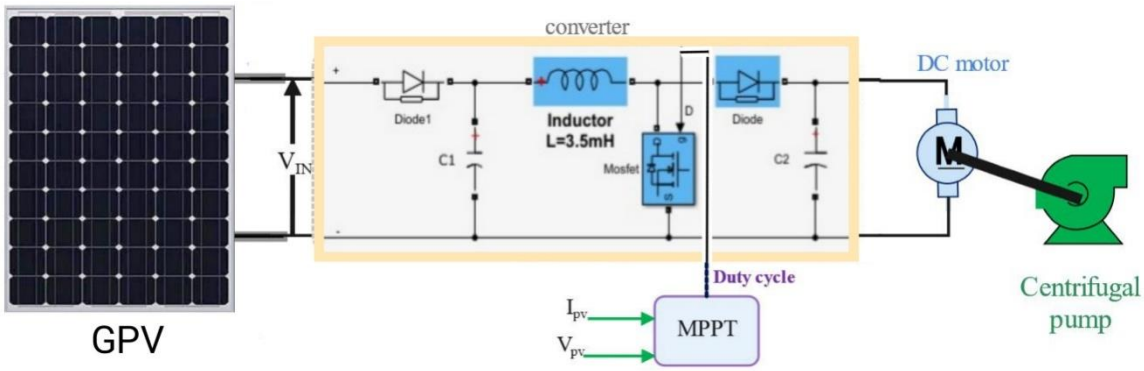

Figure IV-7 SMC MPPT in Solar Power System: Optimizing DC Pump Supply

In the block diagram depicted above, the chopper can transfer maximum power to the load when it operates with the optimal duty ratio, D. The peak power, Ppeak, delivered to the load under steady-state conditions at various solar insolation levels can be determined using Equation (IV.53).

$$P_{peak} = R_a I_a^2 + E I_a \tag{IV.53}$$

The duty ratio is defined in terms of the motor speed to illustrate how the motor speed changes with variations in the buck chopper duty ratio. Hence, Equation (IV.52) can be reformulated in terms of speed. Referring to Equations (IV.50) and (IV.51), the torque produced by the motor under steady-state conditions is determined by either Equation (IV.54) or (IV.55).

$$\frac{E I_a}{\omega_m} = B_m \omega_m + T_L \tag{IV.54}$$

$$E I_a = B_m \omega_m^2 + T_L \omega_m \tag{IV.55}$$

Similarly from Equation (IV.52), the armature current is given by

$$I_a = \frac{B_m \omega_m + T_L}{K_t} \tag{IV.56}$$

Substituting Equations (IV.55) and (IV.56) into (IV.53) yields,

$$P_{peak} = \left(\frac{B_m \omega_m + T_L}{K_t}\right)^2 R_a + B_m \omega_m^2 + T_L \omega_m$$

(IV.57)

$$P_{peak} = \frac{R_a}{K_t^2}\left(B_m{}^2\omega_m{}^2 + 2B_m\omega_m\, T_L + T_L{}^2\right) + B_m\omega_m{}^2 + T_L\omega_m \tag{IV.58}$$

Equation (IV.58) yields a polynomial whose degree is contingent upon the load torque T_L type. By solving Equation (IV.58) for wm across different insolation levels, considering only real and positive values, we ascertain the duty ratio Dvariation with speed wm corresponding to peak powers associated with varying solar insolation levels. This is achieved by calculating the output voltage Vo of the buck chopper from

$$V_o = R_a\, I_a + E = R_a\, I_a + K_e\omega_m \tag{IV.59}$$

Where ωm is the speed corresponding to maximum power point of Equation (IV.58) and then Ia can be obtained by substituting this value of ωm into Equation (IV.56)

$$\left(\frac{B_m{}^2 R_a}{K_t^2} + B_m\right)\omega_m{}^2 + \left(\frac{2B_m(T_p)R_a}{K_t^2} + (T_p)\right)\omega_m + \frac{(T_p)^2 R_a}{K_t^2} - P_{peak} = 0 \tag{IV.60}$$

3.4.4 Centrifugal pump load

Although both volumetric pumps and centrifugal pumps are widely used in PV pumping systems, [33] reported that a DC motor driving a constant volume pump represents a non-matched load for a PV array due to its requirement for nearly constant current. However, [34] found that the energy utilized by a PV array driving a centrifugal pump is significantly higher than that by a volumetric pump. This is because centrifugal pumps operate for longer periods even at low insolation levels, and their load characteristics align well with the maximum power locus of the PV array. Additionally, centrifugal pumps are inexpensive, simple, require low

maintenance, and are available in a wide range of flow rates and heads. Consequently, a centrifugal pump is considered in this work.

The centrifugal pump load generates speed-dependent torques. The speed-torque characteristics of a centrifugal pump, including friction torque, are approximately given by Equation (IV.61) [35].

$$T_p = T_L = A_L K_L \omega_m^{1.8} \tag{IV.61}$$

Tp is the torque required to drive the pump, AL is the load friction (Nm) and KL The proportional constant of the load torque N.m/(rad/sec)2 . Since the load torque TL = Tp , hence Equation (IV.58) becomes:

$$\left(\frac{B_m^2 R_a}{K_t^2} + B_m\right)\omega_m^2 + \left(\frac{2B_m(T_p)R_a}{K_t^2} + (T_p)\right)\omega_m + \frac{(T_p)^2 R_a}{K_t^2} - P_{peak} = 0 \tag{IV.62}$$

$$\left(\frac{K_L^2 R_a}{K_t^2}\right)\omega_m^4 + \left(\frac{2B_m K_L R_a}{K_t^2} + K_L\right)\omega_m^3 + \left(\frac{B_m^2 R_a}{K_t^2} + B_m\right)\omega_m^2 - P_{peak} = 0 \tag{IV.63}$$

Equation (IV.63) is implemented in MATLAB to calculate the rotation speed of the motor ωm for a given value of peak power Ppeak.

IV.5.4 Sliding Mode Control Simulation of the First PV System

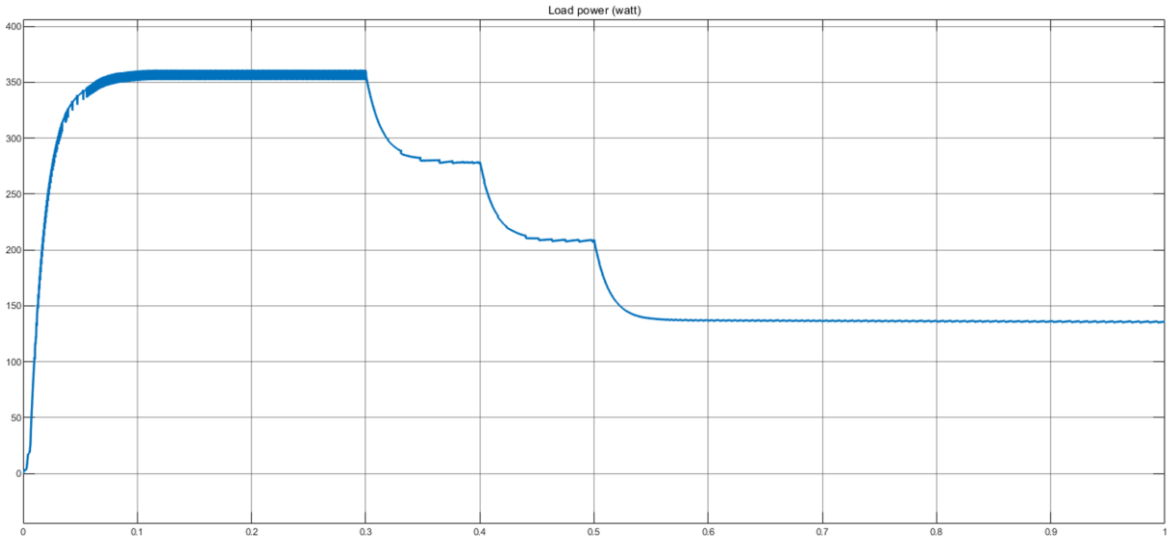

Figure IV-8 Power received by the load

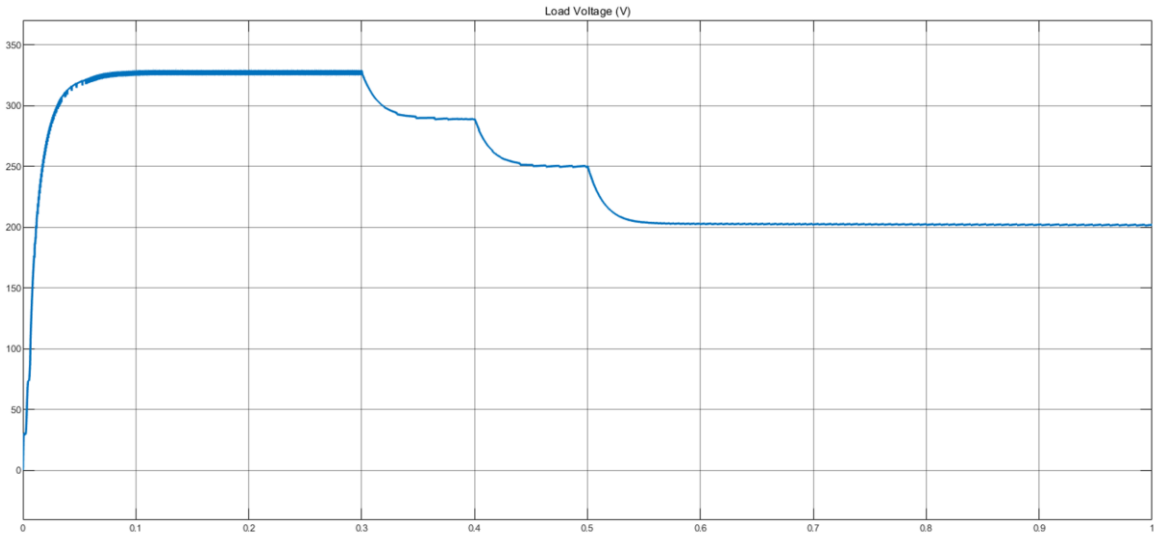

Figure IV-9 Voltage across the load.

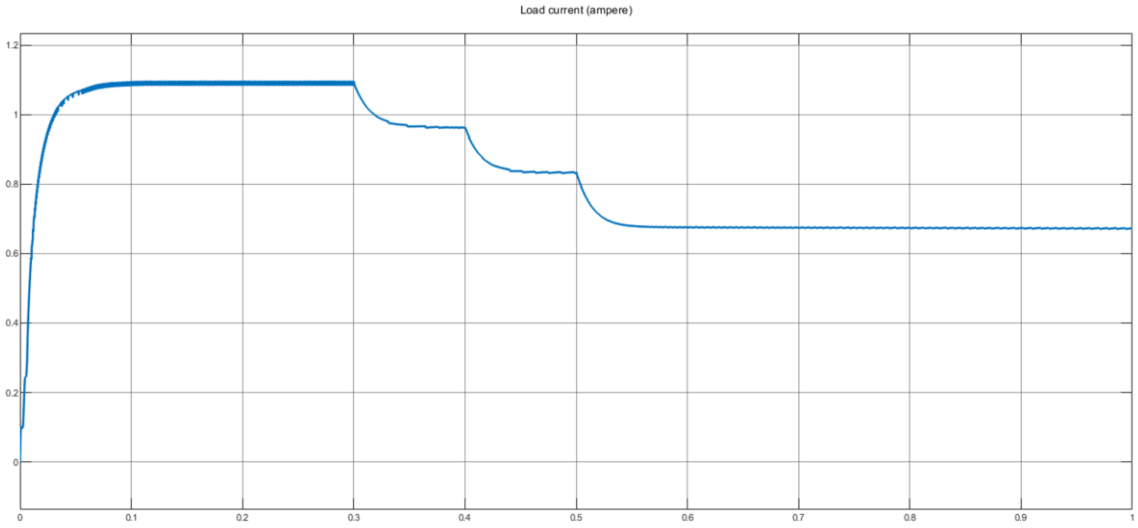

Figure IV-10 current flowing into the load

Discussion

According to the power delivery curve, the PV array reaches its maximum power point very quickly (approximately 0.025s). This demonstrates the speed and efficiency of the proposed sliding mode control. However, we observed the occurrence of chattering in the control and in all system variables (current, voltage, power, etc.). This phenomenon is caused by the sign function of the discontinuous term u_{sw} in the control. Additionally, the constant γ has a significant impact on the chattering and the system's response time. Indeed, minimizing γ reduces chattering, but the system becomes slightly slower. Conversely, increasing γ speeds up the system but results in significant chattering.

IV.6. Conclusion

In this chapter, we presented the theory of sliding mode control initially. This nonlinear control has the advantage of robustness against uncertainties. Its principle is to bring the system to a chosen sliding surface using a discontinuous term, and then to maintain it along this surface using a continuous term, known as equivalent control.

We applied this principle to address the MPPT control problem for a PV system consisting of a PV generator connected to a Buck converter. Finally, we simulated this sliding mode approach

presented in this chapter. Simulation results show that the PV generator converges to its maximum power point quickly. To mitigate the chattering phenomenon, the sign function is replaced by a continuous approximation presented by the hyperbolic tangent function.

General Conclusion

General Conclusion

This research explored photovoltaic (PV) systems and direct current (DC) machines across four main chapters. In the first chapter, we provided an overview of PV energy and DC machines, detailing the fundamental principles and the conversion of sunlight into electricity using semiconductor materials. The second chapter focused on modeling and distribution of PV cells, along with the effects of temperature and solar irradiance on the performance of these cells. In the third chapter, we examined direct and indirect coupling techniques, emphasizing power converters and control using Maximum Power Point Tracking (MPPT) techniques to optimize PV system efficiency. The fourth chapter was dedicated to the principle of sliding mode control, demonstrating its application to PV systems to minimize disturbances and enhance performance. Through this research, we highlighted the critical role of renewable energy, particularly solar energy, in meeting the increasing global energy demand sustainably and environmentally friendly. The findings show that integrating PV systems with DC machines offers promising solutions for achieving energy sustainability. However, realizing these goals requires further advancements in technology and optimization methods to ensure better efficiency and performance.

References

[1] Souilamas, Nesrine, and Krimi, Romaissa. "Study and Simulation of a Thin-Film-Based Structure for Photovoltaics." Master's Thesis, Saad Dahlab University of Blida, 2014.

[2] Zhang, L., Jiang, F.D., Feng, J.Y. "Sol Energy Mater Sol Cells 80:483." 2003.

[3] Al-Bassam, A.A.I. "Physica B 266:192." 1999.

[4] Bouchritte, Wafa. "Multilevel Converters in Grid-Connected PV Systems." Master's Thesis, Mohamed Khider University of Biskra.

[5] Boukli-Hacen, Omar. "Design and Implementation of a Photovoltaic Generator Equipped with an MPPT Converter for Better Energy Management." Doctoral Thesis, Abou Bekr Belkaid University of Tlemcen.

[6] Labouret, Anne, and Villoz, Michel. *Energie Solaire Photovoltaique*. 4th ed., Dunod, Paris, 2009.

[7] Belhadj, Mohammed. "Modeling of an Autonomous Photovoltaic Capture System." Master's Thesis, University Center of Bechar, 2008.

[8] Meekhum, Dariga. "Implementation of a Conversion and Energy Management System for a Photovoltaic System to Power Autonomous Wireless Sensor Networks for Aeronautical Applications." Doctorate in Electrical Engineering, University of Toulouse.

[9] Bessemoulin, Pierre, and Olivieri, Jean. "Solar Radiation and Its Ultraviolet Component." Météo-France, Central Meteorology Operations Service Toulouse, La Météorologie 8th Series, No. 31, September 2000.

[10] Hadj Belkacemi, Mohammed. "Modeling and Experimental Study of an Unglazed and Perforated Solar Collector." Master's Thesis, Abou Bekr Belkaid University of Tlemcen, 2011.

[11] Slama, Fateh. "Modeling of a Multi-Generator Photovoltaic System Interconnected to the Electrical Grid." Master's Thesis, Ferhat Abbas University – Setif, 2011.

[12] Benkhelifa, Abdelaziz. "Modeling and Experimental Study of a Planar Water Solar Collector: Influence of Solar Irradiance Intensity and Collector Inclination on Collector Efficiency."Master's Thesis, Kasdi Merbah University of Ouargla, 2012.

[13] S.Mameri. M.Leghima. «Asservicement de vitesse d'un moteur à courant continu». Mémoire de Master. Université Tizi-Ouzou .2018.

[14] B.Equer, «Le Pompage Photovoltaïque Manuel de cours », énergie solaire photovoltaïque ellipses 1993.

[15] K.Benlarbi « Optimisation Floue, Neuronale et Neuro-Floue d'un système de Pompage Photovoltaïque Entraînées par différents machines électriques »Thèse de Magister, Université de Batna 2003.

[17] Bessam-Abdelghani, Modélisation et Simulation d'un pompage photovoltaïque, Mémoire de magister, Badji Mokhtar- ANNABA University 2018 [18] Afghan, Syeda Adila & Abdul Kareem, Hassam & Hussy, Gaza. (2017). Simulating the electrical characteristics of a photovoltaic cell based on a single-diode equivalent circuit model.

[19] Alternative Energy Tutorials, Web 19 June 2021 https://www.alternative-energy-tutorials.com/photovoltaics/bypass-diode.html

[20] Electronic tutorial, Web 19 June 2021

https://www.electronics-tutorials.ws/diode/bypass-diodes.html

[21] DJERIOU Salim, Performance Improvement of photovoltaic pumping system, PhD Dissertation, University M'Hamed BOUGARA – Boumerdes 2018, Page 27

[22] T. S. Akassewa, «Système d'alimentation photovoltaïque avec stockage hybride pour l'habitat énergétiquement autonome», thèse doctorat, Université Henri PoincaréNancy, 2010.

[23] S. Abada, «Etude et prtimisation d'un générateur photovoltaique pour la recharge d'une batterie avec un convertisseur sepic», Thèse de doctorat, Université du Laval, QUEBEC, 2011.

[24] R. Shubhobrata, B. Ranjit Kumer et M. Maitra, Singapore, Block Backstepping Design of Nonlinear State Feedback Control Law for Underactueted Mechanical systems, Springer, 2016.

[25] J.J.E. Slotin et W. Li, APPLIED NONLINEAR CONTROL, Prentice Hall,

Englewood Cliffs, NJ, 1991.

[26] V.Bregeault, "Quelques Contributions À La Théorie De La Commande Par Modes Glissants", these de doctorat, Université de Nantes, 2013.

[27] V. I. Utkin, «Sliding Mode Control Design Principles and Applications to Electric Drives» IEEE Transactions on Industrial Electronics, Vol 40, No 1, pp. 23-36, 1993.

[28] J. P. Barbot et W. Perruquetti, New York, Sliding Mode Control In Engineering,

MARCEL DEKKER, INC. 2002.

[29] M. H. Rashid, Power Electronics - Circuits, Devices, and Applications 3rd Edition Pearson Education: Academic Pr, 2004.

[30] A. O. Omole, "Analysis, modeling and simulation of optimal power tracking of multiple-modules of paralleled solar cell systems," Master of Science Thesis, The Florida State University College of Engineering, 2006.

[31] R. Krishnan, Electric motor drives: modeling, analysis, and control vol. 626: Prentice Hall Upper Saddle River, NJ, 2001.

[32] J. Gonzalez-Llorente, et al., "Analyzing the optimal matching of dc motors to photovoltaic modules via dc-dc converters," in Applied Power Electronics Conference and Exposition (APEC), 2010 Twenty-Fifth Annual IEEE, 2010, pp. 1062-1068.

[33] W. R. Anis and H. M. B. Metwally, "Dynamic performance of a directly coupled PV pumping system," Solar energy, vol. 53, pp. 369-377, 1994.

[34] A. Ghoneim, "Design optimization of photovoltaic powered water pumping systems," Energy conversion and management, vol. 47, pp. 1449-1463, 2006.

[35] J. Appelbaum, "Starting and steady-state characteristics of DC motors powered by solar cell generators," Energy Conversion, IEEE Transactions on, pp. 17-25, 1986.